Voight, B. & Elsworth, D. (1997). *Géotechnique* 47, No. 1, 1–31

Failure of volcano slopes

B. VOIGHT* and D. ELSWORTH*

Magmatic intrusions can initiate and sustain massive and catastrophic volcano collapse. Their role is twofold, involving both driving and resisting forces. First, flank stability is diminished by magmastatic and magma overpressures, and steepened slopes, that accompany intrusion. Second, excess pore pressures in potential failure zones can be generated as a result of intrusion-related mechanical or thermal straining of the rock-fluid medium, pressurized retrograde boiling in high level magma chambers, or hydrothermal fluid circulation. Also, earthquakes may aid collapse through inertial forces and shaking-induced pore pressure generation. These excess pore pressures reduce the sliding resistance, as shown for wedge-shaped slide blocks for selected cases. The destabilizing influence of mechanically induced pore pressures is maximized as the intruded width, or corresponding overpressure, of the intrusion is increased. The destabilizing influence of thermally induced pore pressures is conditioned by the severity of thermal forcing, ratios of thermal and hydraulic diffusivities, and the time required for the fluid pressure disturbance to propagate outwards from the intrusion. Retrograde boiling and hydrothermal circulation overpressure mechanisms may be evaluated by similar models. Failure initiation does not imply sustained failure; in some cases, enhancement of pore pressures through deviatoric shearing, frictional heating, or runout over compressible saturated alluvium or marine sediments may be necessary following slide initiation to maintain the impetus of flank failure for long runout. Models are examined for oceanic volcanoes of shallow flank inclination and for terrestrial composite volcanoes with considerably steeper flanks.

KEYWORDS: Earthquakes; landslides; rocks/rock mechanics; slopes.

Les intrusions magmatiques peuvent provoquer et entretenir l'effondrement massif et catastrophique d'un volcan. Elles le font en faisant intervenir à la fois des forces d'entraînement et des forces de résistance. Pour commencer, les surpressions magmastatiques et magmatiques et l'accentuation des pentes qui accompagnent l'intrusion réduisent la stabilité des versants. Deuxièmement, la pression des pores peut devenir excessive dans les zones d'effondrement potentiel sous l'effet des contraintes mécaniques ou thermiques imposées au milieu roche-fluide par l'intrusion, du bouillonnement rétrograde sous pression dans les réservoirs de magma de haut niveau, ou de la circulation du liquide hydrothermal. Les séismes peuvent, eux aussi, contribuer à l'effondrement en produisant des forces d'inertie et des secousses qui font augmenter la pression des pores. L'excès de pression réduit la résistance au glissement, comme le montrent les exemples de blocs de glissement en coin illustrés dans l'article. Plus l'intrusion est large ou plus la surpression correspondante est forte, plus l'augmentation mécanique de la pression des pores a un effet déstabilisant. L'effet déstabilisant de l'augmentation thermique de la pression des pores dépend de l'importance du refoulement thermique, des ratios de diffusivité thermique et hydraulique, et du temps de propagation de l'augmentation de pression. On peut utiliser des modèles semblables pour évaluer le bouillonnement rétrograde et les mécanismes de surpression de la circulation hydrothermale. L'amorce d'un effondrement n'est pas nécessairement suivie d'un effondrement entretenu: dans certains cas, l'effondrement des versants, une fois amorcé, ne peut se poursuivre que si la pression des pores augmente sous l'effet d'un cisaillement déviateur, d'un réchauffement produit par frottement, ou d'un écoulement sur des alluvions ou des sédiments marins saturés et compressibles. Let auteurs examinent des modèles pour des volcans océaniques à pentes faibles et pour des volcans terrestres composites à versants bien plus raides.

Manuscript received 4 October 1994; revised manuscript accepted 19 October 1995.
Discussion on this paper closes 2 June 1997; for further details see p. ii.
* Pennsylvania State University.

INTRODUCTION

Volcano slope failures range from moderate sized, localized movements of tephra deposits or rock to enormous slope failures involving evisceration of the

edifice (Fig. 1). Some rank among the largest mass movements on earth, and are among the most severe natural hazards that confront humankind. Terrestrial avalanches of 1–10 km^3 in volume have travelled as much as 100 km and have affected areas of up to 1500 km^2 (Siebert, 1984; Siebert, Glicken & Ui, 1987). Some submarine landslides have been larger, with volumes of up to 5000 km^3, travel distances exceeding 200 km, and depositional areas as great as 23 000 km^2 (Moore, 1964; Moore, Clague, Holcomb, Lipman, Normark, & Torresan, 1989). The full spectrum of landslide types may occur, but for convenience most initial movements can be divided into block slides (translational) or slumps (rotational), which often involve episodic lateral movement, and in some cases evolve into unstable, mobile flows. Debris avalanches are typical of such flows and are characterized by the fast movement of large volumes of rock and debris fragments over great distances on low-angle slopes (Voight, 1978, 1979; Moore *et al.*, 1989).

Over 17 major terrestrial slope failures have occurred in the past 400 years. Avalanches accompanied by magmatic explosive volcanism occurred at Mount St Helens, USA, in 1980; Shiveluch in 1854 and 1964 and Bezymianny in 1956, both from Kamchatka; Harimkotan in the Kuriles in 1933; Augustine, Alaska, in 1883; and in Japan, at Oshima-Oshima in 1741 and Komatage in 1640 (Voight, Janda, Glicken & Douglass, 1983; Siebert *et al.*, 1987). Avalanches accompanied by phreatic explosive volcanism occurred at Bandai, Japan, and Ritter Island, Papua New Guinea, both in 1888; Papandayan, Java, in 1772; and Iriga, Philippines, probably in 1628. Numerous gigantic slump movements and avalanches are also recorded for oceanic islands, including the episodically active, magmatically-nudged flanks of Kilauea and Réunion Island volcanoes. Large landslides on volcanic cones unaccompanied by coeval volcanism have been relatively frequent, such as the 34×10^6 m^3 Ontake debris avalanche, Japan, in 1894.

Avalanches may also cause catastrophic waves from interaction with oceans or lakes (Slingerland & Voight, 1979; Siebert *et al.*, 1987), and avalanche deposits may impound hazardous, short-lived lakes (Costa & Schuster, 1988). Obviously, collapsing volcanoes and associated explosions and water waves are extremely hazardous. During the past 400 years more than 20 000 people have been killed by avalanches or closely related events, excluding lahars, which can be even more lethal.

This paper considers the various causes of volcano collapse, and develops a generalized mechanical analysis to establish the qualitative significance of important factors leading to collapse. The role of magma is explored in detail, in relation to its direct influence on the driving forces tending to destabilize the edifice, and also to its indirect influence on pore fluid pressure distribution. The latter affects rock frictional resistance and is shown to be at least of equal importance as a destabilizing factor. Attention is also given to the important destabilizing role of seismicity, and to the indirect role of magma in causing hydrothermal circulation and alteration, and intensive fracturing.

CAUSES OF VOLCANO COLLAPSE

Volcano collapse is always produced by a combination of events or circumstances rather than

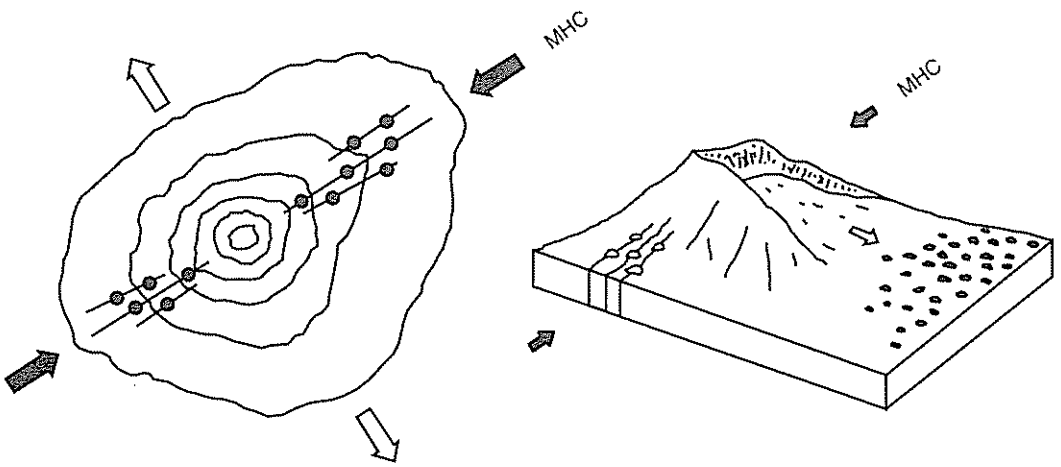

Fig. 1. Preferred emplacement of radial dykes and parasitic cones parallel to the direction of maximum horizontal compression (MHC), producing elongation of the edifice. Flank failure often occurs normal to this direction. Intrusions of similar trend at high level within the edifice apply strong magmatic forces that promote flank failure (after Siebert (1984) and Moriya (1980))

any single process or cause, although in some cases a specific action—perhaps overwhelming or perhaps trivial, depending on whether or not the mass is already on the verge of failure—may set the mass in motion (Voight, 1992). This final action 'triggers' the collapse, but is never the sole cause. An additional complexity is that a 'trigger' process may operate in the short term or with delayed action.

Given the inherent characteristics of materials and conditions, the additional causes of collapse can then by divided into factors that produce an increase in shear stress and factors that contribute to a reduction in shear strength (Table 1). This is the approach of Terzaghi (1950) for conventional landslides (cf. Varnes, 1978; Voight, 1992). In some situations a given action may contribute simultaneously to both a stress increase and a strength decrease, but it is nevertheless useful to separate the physical components in so far as possible. Human-influenced factors are generally relevant only to relatively small events and are neglected in this paper.

For small to moderate sized collapses, the conventional geotechnical approach adequately explains operational processes. Intense and variably-oriented jointing, and physiochemical factors such as hydrothermal alteration to clays and base exchange, may be particularly significant in reducing shear strength (Hoek, 1983; Barton & Choubey, 1977). The conventional causes, such as fluid pressure enhancement related to precipitation or to seismic loading, are then superposed on this gradually weakened material. Slope angle is clearly an important factor in volcano collapse, as indicated by the frequency of major slope failures on steep composite volcanoes compared with shields (Fig. 2; Siebert, 1984).

In some cases, a combination of causative factors related to landslides may operate more or less uniformly over a broad territory. Thus in Ecuador in 1988 (Belloni & Morris, 1991), a regional earthquake created regional dynamic loading of slopes previously saturated by tropical rainstorms. The result was extensive landsliding over a vast region. In other cases, the interaction of several factors may make certain areas more slide-prone than others. Ground subjected to on-average slow (steady or episodic) creeping motions, due to a nearly-critical ambient balance of shear stress and strength, is potentially hazardous. Such 'slow' ground movements may further reduce the strength in the zone of shear, and may also produce open surface fractures that in turn cause increases in water content and the establishment of destabilizing water pressures. This can lead to substantial failure of saturated ground—a type of failure especially dangerous due to the potential for high mobility and rapid motion.

ROLE OF MAGMA IN VOLCANO COLLAPSE

For very large volcano sector movements, the mechanical problem is not yet resolved. In some cases a magmatic driving force seems clearly involved, and indeed the role of magma can be decisive, inasmuch as it directly or indirectly influences many 'causes' that increase shear stress and 'causes' that decrease shear strength; inspection of Table 1 demonstrates the complexity and significance of magmatic involvement. In the remainder of this paper the role of magma is explored in detail.

A strong preferred orientation of the axes of composite volcano avalanche scars has been observed normal to the dominant dyke direction (Fig. 1; Siebert, 1984; Moriya, 1980). Siebert also noted that in Japan, which has the highest documented number of volcano avalanche scars, a much higher percentage of volcanoes with parallel dyke swarms have formed avalanche calderas than have volcanoes lacking a dominant direction of dyke orientation. Elongation of the volcanic edifice also occurs parallel to the dyke trend (Moriya, 1980). Similarly, at Stromboli volcano in the Aeolian Arc, Italy, where the whole history of volcano growth involved a dominant NE–SW orientation of dyke injection and fracturing, comprising a rift zone, three flank collapses followed a preferential NW sliding direction (Romagnoli & Tibaldi, 1994).

These data suggest that a 'dilational effect' of parallel dyke swarms, often related to the regional tectonic stress directions, can be an important factor in major volcanic slope failure. We interpret this effect mainly in terms of the magmatic driving force normal to high-level magma intrusions of the same trend within the edifice, rather than to dilational strains associated with intrusions at low level or beneath the edifice.

At the Kilauea shield volcano, Hawaii, displacement and seismic events on the south flank take place soon after magmatic intrusive activity, indicating that the displacement is caused *by* forceful intrusion in the rift zones, and is not the cause *of* passive intrusion (Swanson, Duffield & Fiske, 1976). Thus the injection of dykes, or other intrusive forms, provides a clear mechanism to assist the initiation of debris avalanches or deep flank slip, by creating a magma wedge that severs the updip attachment of the potential slide block to the volcanic cone, and exerts substantial magma pressure on the head wall (Voight, 1972, 1974; Gueva & Kehle, 1978; Prostka, 1978). The basic idea is very old and may be traced to James Hall (1815). A magmatically augmented driving force has been proposed as a cause of lateral slip in Hawaii (Lipman, Lockwood, Okamura, Swanson & Yamashita, 1985; Dieterich, 1988), although for Hawaii the mechanisms both of failure and of long runout have appeared 'mechanically enigmatic'

Table 1. Causes of volcano collapse

Inherent causes

1. Initial composition
2. Texture—loose, porous, weak materials are slide-prone
3. Bedding attitude relative to slope face
4. Layering sequences in relation to strength and permeability
5. Discontinuity systems—faults, joints, dykes, bedding planes
6. Slope forming process history, movement history; bedding slip and fault slip history and orientation of movement
7. Initial physicochemical setting; conditions of weathering and alteration
8. History of seismicity and seismic damage
9. Ambient (seasonal) groundwater conditions

Causes that increase shear stress

1. Removal of lateral or underlying support of slopes
   (*a*) Erosional processes producing, steepening, or undercutting natural slopes
   (*b*) Prior mass movements
   (*c*) Phreatic explosions near base of slope
2. Static loading
   (*a*) Natural deposition—slope or river sedimentation, tephra, lava
   (*b*) Weight of water added by natural precipitation or by exsolved volatiles
   (*c*) Seepage pressures and joint water pressures
   (*d*) Magma pressure
   (*e*) Swelling pressures in expansion clays
3. Dynamic loading
   (*a*) Regional or local tectonic earthquakes
   (*b*) Vibrations from volcanic earthquakes, explosion and eruptive processes
   (*c*) Vibrations from adjacent, rapidly-moving landslides
4. Increase of surface slope
   (*a*) Magma-intrusion-related deformation (cryptodomes)
   (*b*) Regional tectonics (slow or episodic change)
   (*c*) Slope changes due to depositional processes

Causes that reduce shear strength

1. Physicochemical factors
   (*a*) Hydrothermal alteration
   (*b*) Softening of clays
   (*c*) Hydration of clay minerals
   (*d*) Ion exchange of clays
   (*e*) Weathering
   (*f*) Solution of grain cement
   (*g*) Decomposition of organic materials
   (*h*) Physiocochemical fracturing
2. Pore fluid pressure enhancement
   (*a*) Heavy rainfall or rapid snowmelt
   (*b*) Changes in groundwater flow regime
   (*c*) Pore-pressure changes in aquifers adjacent to magma intrusion, due to poroelastic deformation, thermal expansion, or separation of gas from magma chambers
   (*d*) Pore-pressure changes due to hydrothermal processes
   (*e*) Thermal expansion of pore fluid due to frictional slip
   (*f*) Vibration-induced pore fluid pressure rise
   (*g*) Shear deformation-induced pressure rise
   (*h*) Consolidation seepage induced by surcharge
   (*i*) Base level change in reservoirs, lakes or oceans
   (*j*) Flow boundary condition changes (e.g. iced or plugged flow egress points)
   (*k*) Enhanced glacier melting due to increased geothermal flux
3. Changes in structure
   (*a*) Disturbance, remoulding
   (*b*) Particle reorientation due to slip or dynamic loading; peak to residual strength loss
   (*c*) Grain collapse in altered, weakened tephra deposits
   (*d*) Fracturing and loosening of valley walls, stress relief, etc.
   (*e*) Deep-seated fracturing associated with magma intrusion, stress relief, geothermal processes, physiochemical alteration
   (*f*) Adjustments to groundwater flow paths; slope drainage enhanced or impeded

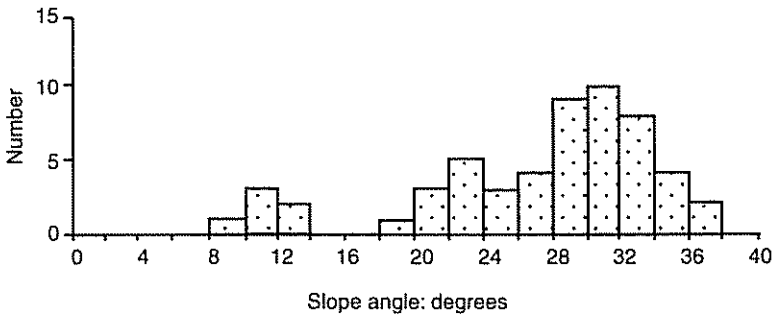

Fig. 2. Slope angle of Quaternary volcanoes associated with major flank failure

because of frictional resistance (Iverson, 1991). Thus even a formidable magmatic driving force is insufficient to explain movements of a block kilometres thick and 10^2 km long on a relatively flat slope with conventional friction coefficients. As subsquently demonstrated, the situation for stratovolcanoes may be less severe than for shield volcanoes because of the steeper slopes.

The problem for Hawaii is partly analogous to the 'overthrust problem' posed by structural geologists a generation ago (Hubbert & Rubey, 1959; Voight, 1976), and the resolution proposed is similar—in order to enable movement of a slide block of the appropriate dimensions, it is necessary to reduce drastically the frictional resistance of the basal slide plane. The most likely mechanism for this is by enhanced pore fluid pressures in conjunction with the Terzaghi principle of effective stress.

The question that next arises is how to explain the required rise in pore fluid pressure. Iverson (1992, 1995) considered several conditions 'under which large scale failures might occur', including gravity driven hydraulic gradients, sea-level changes, and gravitational consolidation due to a growing volcano mass, possibly in combination with magma pressure. He concluded, however, that these mechanisms were insufficient to cause large-scale failure, and therefore 'a simple quantitative explanation for the failure of Hawaiian volcano flanks remains elusive'.

The authors hypothesize that the pressurization of pore fluids accompanying magmatic intrusion can be a sufficient additional trigger mechanism for volcano collapse (Voight & Elsworth, 1992). The fluid pressurization mechanisms directly associated with magmatism include

(*a*) pore pressures developed mechanically in porous elastic media around rapidly-intruded dykes
(*b*) thermal expansion of aquifer pore fluids heated by intrusions or (more efficiently) by eruption feeder dykes, accompanied by long-distance lateral pressure transmission within the aquifer (e.g. Delaney, 1982)
(*c*) pressurized volatile separation in high-level intrusions, in association with cooling, crystallization, and retrograde boiling processes, leading to hydrofracturing and/or 'steam-drive' pressure transmission in adjacent or superjacent aquifers.

Other mechanisms may be indirectly associated with magmatism

(*d*) hydrothermal system overpressurization mechanisms, producing piezometric head exceeding hydrostatic
(*e*) shaking-induced pore-pressure generation, by volcanic (or tectonic) earthquakes.

Thus magma intrusions can have two effects: to increase the driving force by way of direct magma pressurization or intrusion-related seismic inertial force, and/or to decrease the resisting force by way of fluid pressure enhancement. Pore pressures due to poroelastic deformation may be more rapidly transmitted than those due to thermal expansion or degassing (Elsworth & Voight, 1992, 1995), but the latter processes may be longer lasting and ultimately more effective in provoking volcano collapse. These mechanisms are not hypothetical, as pore fluid pressurization in association with volcanic activity has been observed or monitored at several localities (Björnsson, Kristjánson & Johnson, 1977; Stefánsson, 1981; Watanabe, 1983). The episodes of fluid pressurization cited above appear to have resulted from the mechanical and thermal strain fields induced in saturated porous volcanic materials by magmatic intrusions.

Such pore pressure components may act additively on potential basal failure planes, with the net effect of decreasing Terzaghian effective stresses and consequently decreasing the frictional resistance to failure. In addition, pore pressures generated by intrusions may trigger or amplify moderate to large earthquakes, and these in turn may further aid the processes of flank slip through

shaking-induced pore pressure generation, and ground acceleration that augments the driving force. The interaction of these processes is illustrated schematically in Fig. 3.

These agents of pore-pressure generation provide a rational, and quantifiable, means of sustaining the reduction in basal shear strength, even as the driving forces provided by magma pressurization ultimately drop as flank displacement occurs. Other mechanisms acting within the volcano, such as indirect magmatically related hydrothermal alteration weakening and pervasive fracturing and deformation of the edifice, may also contribute to initial collapse. Mechanisms such as shear-induced generation of pore pressures (Skempton, 1954), frictional-heat fluid pressurization (Voight & Faust, 1982), and limited liquefaction due to granular collapse of weak altered tephra deposits may also act following slide initiation to maintain the impetus of flank failure and accelerate the process. The role of these mechanisms in initiating and sustaining failure is now examined.

MODELS FOR PORE FLUID PRESSURE GENERATION

Pore fluid pressures mechanically generated by intruding dyke

Magma intrusion within a saturated porous medium induces strains in the host medium. These strains cause changes in pore fluid pressures that may dissipate with time, a behaviour that may be approximated by a moving volumetric dislocation (Cleary, 1977, 1978; Rudnicki, 1981). This approach has been applied to the pore pressure fields that were induced by intrusive events at Krafla volcano, Iceland (Elsworth & Voight, 1992).

The volumetric dislocation may be a moving point or line dislocation, representing the geo-

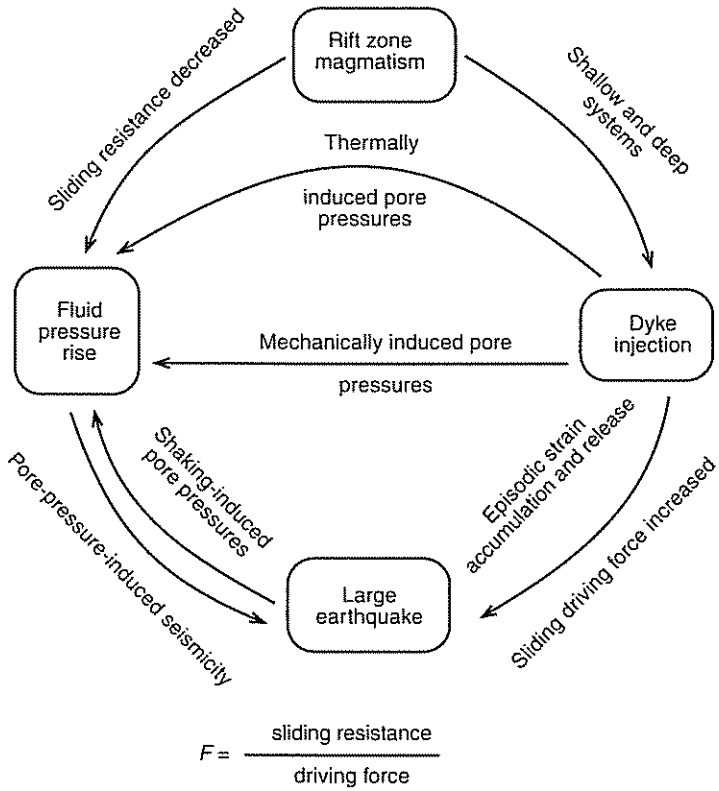

Fig. 3. Influence of dyke intrusion on flank stability. Intrusion induces mechanical and thermal (or hydrothermal) strains that operate on fundamentally different time-scales. These strains, or pressurized volatile separation, induce fluid pressures that may precipitate shallow or deep-seated failure by reducing sliding resistance. Similarly, the magnitude of seismic energy release and its associated destabilizing influences may be enhanced by mechanically or thermally induced pore pressure mechanisms, and by forceful intrusion

metries of pencil or semi-infinite planar dykes respectively. The pore-pressure distributions for these idealizations bound the behaviour of intermediate geometries.

For both the pencil and semi-infinite planar dykes, the induced pore fluid pressures reach a steady state when viewed relative to the migrating dislocation or dyke front. The velocity of dyke propagation is important in defining the morphology of the induced pressure bulb around the dyke front; the physical situation differs considerably from the case where instantaneous intrusion is assumed. For brevity, the planar form is selected as most representative of the geometry of an intruded volcano flank.

For a planar dyke migrating in the x direction and of infinite extent in the y plane (Fig. 4), the steady pressure distribution developed around the

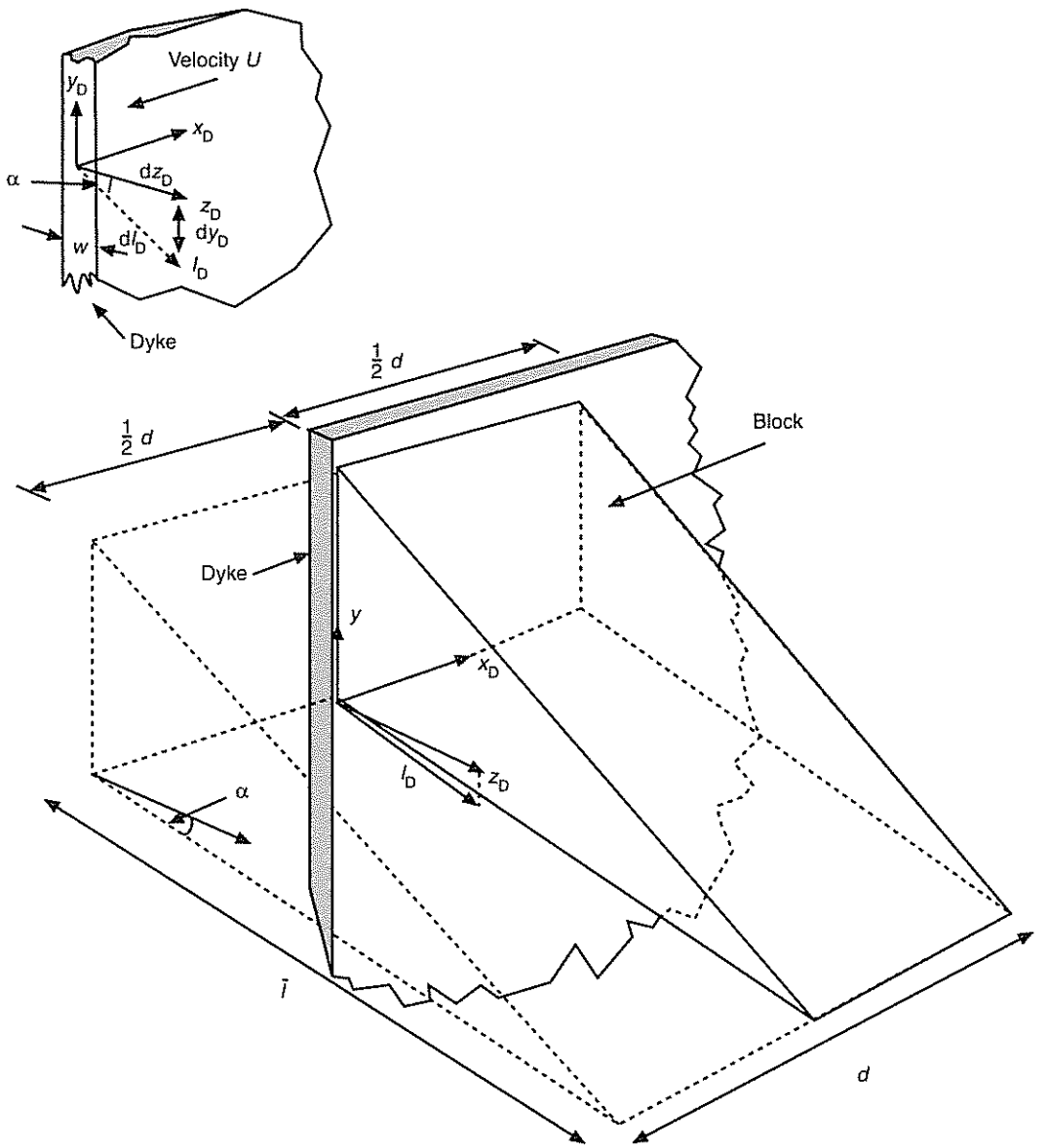

Fig. 4. Geometry for an advancing dyke front at $x_D = 0$ and with a co-ordinate system that migrates with the moving dyke front. The dyke width is w and the front moves with velocity U. Mechanically induced pressures are desired on a plane inclined at α degrees to the horizontal z-axis. The limits of integration are the extent of the plane, given as 0 to l_D and $-\frac{1}{2}d_D$ to $+\frac{1}{2}d_D$

advancing dislocation front is given as (Elsworth & Voight, 1992)

$$P_D^m = K_0^*(U_D R_D)\, e^{U_D x_D} \tag{1}$$

where $K_0^*[x]$ is the modified Bessel function of the second kind of zero order and the mechanically generated dimensionless pressure P_D^m is controlled by the dimensionless intrusion velocity U_D and geometric variables R_D and x_D illustrated in the geometry of Fig. 4. These variables are defined as

$$P_D^m = \frac{2\pi(p - p_s)}{Uw}\frac{k}{\mu} \tag{2}$$

$$U_D = \frac{Uh_s}{2c} \tag{3}$$

$$(x_D, y_D, z_D) = \frac{1}{h_s}(x, y, z) \tag{4}$$

$$R_D^2 = x_D^2 + z_D^2 \tag{5}$$

The parameters that make up these dimensionless groups are width of the intruded dyke w, initial pore fluid pressure p_s, total pore fluid pressure following intrusion p, propagation velocity of the dyke front U, permeability of the porous medium k, dynamic viscosity of the saturating fluid μ, and hydraulic diffusivity of the porous medium c. An arbitrary length parameter h_s, defined in Fig. 7, represents the diffusive length scale and comprises the block crest height above sea-level or above the toe of the failing block. The pore-pressure distribution remains constant with time, relative to the co-ordinate system that migrates with the dislocation front.

Of primary interest is the distribution of induced fluid pressure on a plane inclined relative to the dyke. For failure of a plane section within the y_D–z_D plane, the pressure distribution of interest is that on trace l_D inclined at angle α with respect to the z_D direction (Fig. 4). The normalized trace length is $l_D^2 = y_D^2 + z_D^2$ with $l_D = l/h_s$. The angle is defined as positive counterclockwise from the positive z_D axis. The uplift force F_{pm} acting along this trace is given by integrating the pressure distribution of equation (1)

$$F_{pm} = \int_{-\frac{1}{2}d}^{+\frac{1}{2}d}(p - p_s)\,dl\,dx$$

$$= w_D U_D \gamma_w h_s^3 \int_{-\frac{1}{2}d_D}^{+\frac{1}{2}d_D}\int_0^{\bar{l}_D} P_D^m\,dl_D\,dx_D \tag{6}$$

where

$$w_D = \frac{\mu}{k}\frac{wc}{\pi\gamma_w h_s^2}$$

and the non-dimensional block width d_D is defined as d/h_s, where d is the real block width (see Fig. 4 and 8) and h_s is the height of the block crest above sea level or the block toe. Dimensionless dyke thickness is represented by w_D since, for a given intrusion location, all other parameters are fixed material properties. It is also possible to evaluate the length, $\bar{l}_D^{95}$, required such that 95% of the maximum uplift force is realized

$$\bar{l}_D^{95} \approx \frac{2{\cdot}186}{U_D \cos\alpha} \tag{7}$$

Where the dimensionless trace length is sufficiently large that $\bar{l}_D$ conforms to the requirements of equation (7), the dimensionless uplift force may be determined as illustrated in Fig. 5.

Pore fluid pressures thermally generated by an intrusion

Thermal loading due to intrusion emplacement induces fluid pressures in host rocks. A one-dimensional model may be used to evaluate the approximate pressure distribution on a trace inclined at any angle α to the dyke orthogonal. A simplified expression is available from Delaney (1982) for the case where thermal transport is diffusive and results from the application of a temperature change of magnitude ΔT applied at

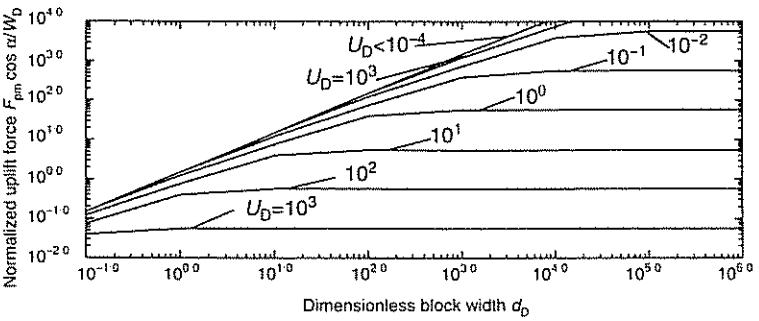

Fig. 5. Integrated uplift force F_{pm} as a function of dimensionless dyke width d_D and dimensionless intrusion rate U_D (evaluations assume $l_D \to \infty$ and the distribution is not truncated along the length)

$z = z_D = 0$. Under this condition, the change in dimensionless pressure P_D^t due to thermal effects alone is given as

$$P_D^t = erfc\left(\frac{Dz_D}{t_D}\right) \tag{8}$$

where D is the ratio of the thermal diffusivity and advective hydraulic diffusivity of the medium and t_D is dimensionless time, with other parameters defined as

$$P_D^t = \frac{(p - p_s)}{K_b A^* D} \tag{9}$$

$$D = \sqrt{\left(\frac{\kappa n}{c}\right)} \tag{10}$$

$$t_D = \frac{4\kappa t}{h_s^2} \tag{11}$$

and K_b is the undrained bulk skeletal modulus of the solid, A^* is thermal strain $\alpha_t \Delta T$, α_t is the coefficient of free thermal expansion, κ is thermal diffusivity, n is porosity, t is time, c is hydraulic diffusivity and z_D is the dimensionless lateral distance from the intrusion, as $z_D = z/h_s$.

This study ignores the convective transport that results from thermal strain, from transfer of gas exsolved from magma into groundwater, or from the fluid pressure gradients mechanically induced by intrusion. These assumptions appear reasonable for a porous medium where pressure gradients remain moderate and Peclet numbers remain considerably less than unity, where Peclet number is the ratio of advective to diffusive thermal fluxes. This condition may be violated close to the intrusion, where the thermal front may induce large pressure gradients and where mechanical strains may be large (Ylinen & Elsworth, 1991). However, the assumption of diffusive-only transport yields a lower pressure change than actual, suggesting that slopes may be less stable than evaluated through this analysis.

The diffusion-induced pressure rise represented in equation (8) is appropriate only for small magnitudes of the material parameters A^* and D (Delaney, 1982). For the geological systems under consideration D is much less than unity. The thermally induced fluid expansion in the porous medium, as conditioned by A^*, is sufficiently large that the original assumptions engendered in equation (8) may be violated. However, comparisons between complete and simplified representations suggest that the underprediction of pressure in the simplifed system is less than 20% (Delaney, 1982), and lithostatic limits on maximum pore-pressure magnitudes will reduce this differential further. Therefore the simplified representations of thermally induced pore pressures are considered appropriate for a first order estimate of uplift force, as follows

$$F_{pt} = dA^* K_b \sqrt{\frac{4\kappa t}{\pi}} \frac{1}{\cos\alpha} \tag{12}$$

or in non-dimensional form by dividing through by $\gamma_w h_s^2$, yielding

$$\bar{F}_{pt} = d_D \frac{A_D}{D} \sqrt{\left(\frac{t_D}{\pi}\right)} \frac{1}{\cos\alpha} \tag{13}$$

$$A_D = \frac{A^* K_b D}{\gamma_w h_s} \tag{14}$$

where the new dimensionless groupings represent the fluid volume generated by the temperature change A_D and the ratio of thermal to advective hydraulic diffusivities D.

Pore fluid pressures generated by retrograde boiling

A body of hydrous magma emplaced within colder host rocks loses heat to its surroundings. As cooling and crystallization proceed, volatile separation occurs according to the reaction: H_2O-saturated melt → crystals + volatile phase. An associated increase in volume is directly proportional to the H_2O content at saturation, and inversely proportional to pressure. At shallow depths such volume increases are large (volume increase > 15% for depth < 4 km, for a dacite (granodiorite) magma with 2·7 weight % H_2O (Burnham, 1979)). Thus H_2O-pressure can also be large, limited only by the strength of wallrock in tension. Under rigid confinement water pressures could theoretically attain several thousand bars, but the tensile strength of wall rocks is at most several hundred bars, and this places a practical upper limit on the achievable magnitude of fluid pressures.

As a consequence of the above, a complex overlapping network of hydraulic fractures surrounds the magma body. Each fracture is propagated more or less radially from the cooling magma, with the direction of local fracture propagation related to local trajectories of principal stresses and to material anisotropy, both of which may be complex.

For high-level intrusives, such pressurized hydrofractures may intersect confined aquifers, and could generate pressure transfer within these aquifers. A one-dimensional model may be used to evaluate the approximate induced pressure distribution, much as reckoned for the case of thermal loading. In more extreme cases, with appropriate stress distribution and anisotropy, hydrofracture orientation may become subparallel to the potential surface of sliding. In this case the pressurized

hydrofracture may itself become a component of the sliding surface.

Due to these various complications, the general representations of uplift force due to thermally induced pore pressure, as described above, are also considered adequate for a first-order estimate of behaviour for the 'retrograde boiling' mechanism. The analogy is approximate and is considered with this limitation in mind. Under extreme circumstances, the associated fluid pressure may be great enough to cause frictional resistance to vanish along the slide plane.

Pore fluid pressures generated by hydrothermal systems

Hydrothermal eruptions occur where the vapour pressure of geothermal fluids exceeds the boiling pressure for a given temperature. The same conditions create subsurface overpressures that can contribute to volcano collapse.

Typically, pressurization occurs where the convective flow of geothermal fluids is impeded by a relatively impermeable cap. The cap is often formed in host rock by silica or carbonate precipitation from geothermal fluids. The vapour pressures of geothermal fluids are also significantly dependent on concentrations of dissolved CO_2 and H_2S, as well as H_2O (Wohletz & Heiken, 1992). Because their sublimation temperatures are lower than for water, vapour pressures can be increased to several tens of bars more than the pore water at any temperature (Kieffer, 1982; Nelson & Giles, 1985).

Examples are shown in Fig. 6, after Hedenquist & Henley (1985) and Wohletz & Heiken (1992). The first involves a shallow hydrothermal reservoir at 200 m depth, with temperature 195°C. The second is for a reservoir twice as deep, with temperature 230°C. In both models a sealed caprock has developed at 100 m depth.

As a result of cap sealing, fluid flow is diverted but vapour accumulates below the cap and above the liquid-water surface table, and gas pressure from greater depth is transmitted to the cap. For the shallow reservoir, the transmitted gas pressure marginally exceeds lithostatic pressure. For the deep system, gas pressure can exceed lithostatic pressure; this pressure is sustained by the strength of the reservoir and cap rock. In both cases, the fluid pressures are in excess of hydrostatic, and can contribute to slope failure if the overpressured system develops under a sloping ground surface. The critical locus of failure is expected in weak layers underlying the cap seal. Transfer of overpressures to higher weak layers in the system is also possible, if the caprock seal breaks by chemical dissolution, preliminary landslide movements (creep rupture), seismogenic fractures or hydrofracturing.

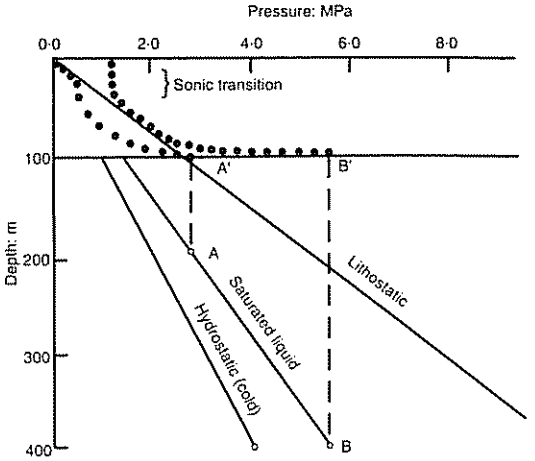

Fig. 6. Pressure–depth relations for hydrothermal reservoirs under an impervious cap at 100 m depth. Pressures with depth of rock overburden (lithostatic), cold vapour-unsaturated water (hydrostatic) and hot vapour-saturated water (saturated liquid) are indicated. The saturated liquid curve shows vapour pressure transmitted from a hot underlying reservoir. The first model for shallow reservoir at 195 °C shows pressurization history by a dashed line (A–A′). A gradual buildup of vapour pressure under the impervious cap continues until its failure, at which time steam may erupt through a conduit with choked flow and emerge at atmospheric pressure (dotted line). For the second model (B–B′) of a deep reservoir, the transmitted vapour pressure greatly exceeds lithostatic pressure at the cap. Ensuing eruptions may be overpressured and supersonic as they emerge from a vent (dotted line), with vent erosion causing the entrainment of lithic ejecta in expanding fluids. In either case, fluid pressures beneath the cap equal or exceed lithostatic pressure, and promote volcano flank failure; slope failure would be accompanied by hydrothermal eruptions that could influence the evolution and final configuration of the avalanche/eruption scar

Hydrothermal (phreatic) eruptions can also occur with caprock failure. Slope failures triggered by hydrothermal pressurization will rupture and unload the hydrothermal system under the caprock, and thus promote a hydrothermal eruption that may be quite violent, depending on the thermodynamic conditions and level of pressurization.

This may have been the circumstance at Bandai volcano in Japan in 1888, where a series of violent hydrothermal eruptions, the last projected almost horizontally, accompanied retrogressive slope failure and the emplacement of a 1·5 km^3 debris avalanche (Sekiya & Kikuchi, 1889). The avalanche buried several villages and blocked river drainages to form five new lakes, and over 450 people perished.

Pore fluid pressures and strength reduction generated by seismicity

Field observations and laboratory tests have demonstrated that earthquake shaking can cause pore water pressure to build up in a saturated material as a result of mineral particles being rearranged with a tendency toward closer packing. If the water cannot drain from the material during straining, gravity loading is transferred from the mineral skeleton to the pore fluid, with a consequent reduction in the capacity of the material to resist shear loading.

Several mechanisms can account for loss of strength of slopes as a consequence of earthquakes. First, if the strained material remains at constant volume, failure can occur only if the material is sufficiently loose for its steady-state undrained strength to be less than the value required to hold the applied forces in equilibrium. This has been termed a type I undrained stress–strain behaviour, defined by a peak followed by a steady-state strength that is lower than its pre-shear consolidation value of shear stress (Castro & Poulos, 1977). A progressive failure can occur with no volume change.

Type II stress–strain behaviour under undrained monotonic shear consists of the resistance *rising* to a steady-state value after large strain. The pore pressure may decrease to counteract the tendency of the material to dilate. In such materials cyclic loading may cause permanent strain and downslope movement, but at the end of transient loading the static stress is less than the peak shear resistance, and movements will be arrested.

Second, if effectively impervious material overlies a granular layer such as tephra, the granular layer *as a whole* must remain at constant volume during undrained cycling loading. However, grains broken or rearranged by cyclic straining may settle individually. With major changes in structure, granular settling may result in the development of a water film near the upper layer interface. Slope failure could obviously be aided by such a condition.

The process involves inhomogeneous redistribution of void ratio within the granular layer—loosening of the upper portion and densification of the lower portion, causing local upward segregation of water. The result is a drastic reduction in the steady-state undrained strength, and vanishing strength if a thick water film develops at the layer boundary and sustains the full weight of overburden. In the limit, frictional resistance may wholly vanish along the sliding surface.

Such a redistribution of void radio has been observed in laboratory tests (Castro, 1975; Gilbert, 1984), and this mechanism may have led to the major slope failure in 1984 at Ontake volcano, Japan, triggered by the Naganoken-Seibu earthquake (Oyagi, 1987; Voight & Sousa, 1994). Here, changes in void ratio within a porous tephra layer were aided by hydrothermal weakening of pumice lapilli; cyclic loading could have ruptured the weakened pumice particles, causing collapse of the granular skeleton and segregation of water layers. Rapid acceleration to high velocity occurred in this mobile, long runout slide.

Third, excess pore fluid pressures in selected granular layers will tend to diffuse into surrounding materials, thus also reducing their shear resistance. The pore pressures migrate more rapidly than would be calculated by simple diffusion through granular pore space, due to enhanced permeability from pressure-enlarged fractures. Excess pressures may also cause hydrofractures and clastic slurry intrusions into adjacent cohesive layers, as well as 'clastic volcano' extrusions. The result of this process is a general reduction in strength of a large volume of material. Thus in addition to decrease of the total shear resistance along potential failure surfaces, global changes of void ratio occur in materials surrounding the granular layers in which the excess pore fluid pressure originated. Under such circumstances the transformation of apparently strong, initially cohesive materials into a mobile avalanche may occur rapidly, as for instance observed for slope failures at Mount St Helens (Voight *et al.*, 1983) and Ontake volcanoes (Voight & Sousa, 1994).

MODELS FOR SLOPE FAILURE

Geometry

Translational displacement of a single wedge (Fig. 7) is an appropriate mode of failure (Dieterich, 1988; Iverson, 1991), and is emphasized in this study. The wedge is bounded at the rear by a planar dyke, of height h_m, and at the base by a potential failure plane of arbitrary inclination α. For oceanic volcanoes the slope geometry incorporates a sea level, at height h_s below the apex of the slope, and a groundwater surface climbing from sea level at an angle θ. The slope angle is defined as β and the geometry is characterized by wedge width d (Fig. 8). For subaerial volcanoes, h_s is reckoned to the toe of the slide wedge.

These geometric parameters determine the magnitude of forces acting on the free-body of the wedge. For oceanic volcanoes the pressure applied to the wedge by seawater is assumed to vary linearly with depth and is given by the product of depth below sea level and unit weight of water γ_w. The total force acting normal to the submarine surface of the wedge is defined as F_s (Appendix 1). The uplift pressures acting on the base of the wedge are defined by the hydrostatic heads acting at the dyke contact and toe. These magnitudes are defined according to Fig. 7 as $b\gamma_w$

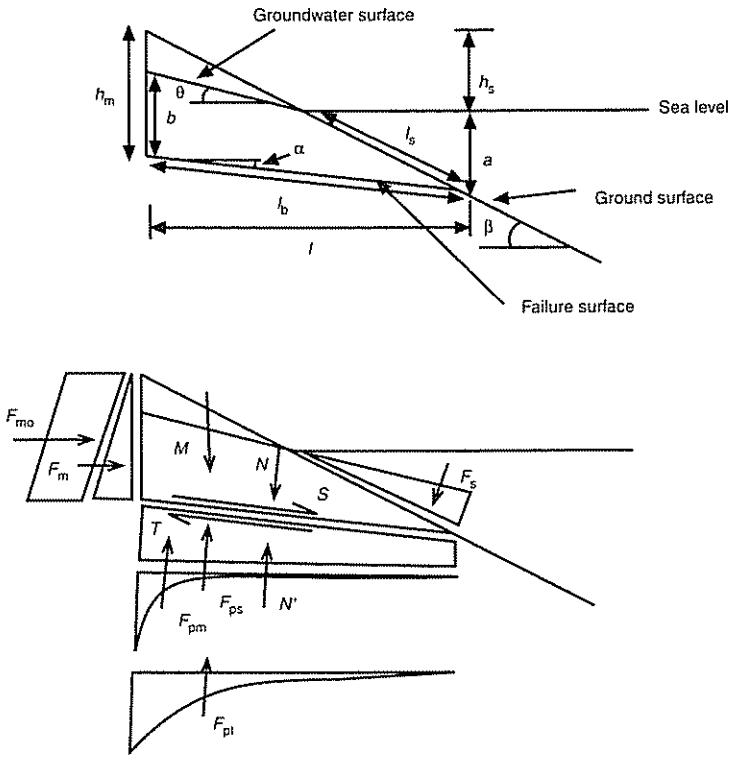

Fig. 7. Generalized geometry for limit equilibrium analysis and identification of parameters. All quantities are defined as positive. α is negative for shallow failure, as treated in this paper. Forces acting on the system are block weight M, seawater pressure F_s, magma force F_m, overpressured magma force F_{mo}, static groundwater force F_{ps}, and induced pore-pressure forces that result from mechanical F_{pm} and thermal F_{pt} strains. N (and its counterforce N') are effective forces normal to the failure surface. The total force driving wedge movement is S, and the mobilized resisting force is T

and $a\gamma_w$ respectively; the difference in unit weights of seawater and freshwater are negligible and are ignored. A linear variation in uplift pressure contributes to the static uplift force F_{ps}. This is reasonable for inclined failure planes that 'daylight' well below sea level, but less realistic for those that daylight at sea level. For the latter, a parabolic distribution would be more appropriate. With the linear distribution the resulting calculation yields a slightly higher factor of safety than for the parabolic distribution.

The analysis is defined in terms of effective stresses. The total stress distributions illustrated in Fig. 8 are used to determine the magnitude of the lateral force F_l resulting from earth pressure at rest. For simplicity, intrusion-induced pore fluid pressures are not subtracted from the assumed total stress distribution, although static groundwater pressures are. This simplification yields slopes that will be generally less stable in reality than predicted.

The average unit weight of the material comprising the failing wedge is defined as γ_r. The strength along the potential failure surface is assumed to be characterized by a single value of friction angle ϕ. Where the cohesive strength of the material is significant, as for instance for the linear approximation of a segment of a non-linear shear strength against effective normal stress relationship, this may be readily incorporated by using an 'apparent' friction angle ϕ, with zero cohesion. The effective frictional resistance will, in general, be normal–stress dependent, and must be averaged over the length of the basal failure plane.

Lateral magma pressure from a planar dyke intruded behind the buttressing wedge is decomposed into two components. The first is the lateral pressure resulting from the static magma column, assumed to vary linearly with depth. The lateral force resulting from the static column F_{ms} is given as $F_{ms} = \frac{1}{2}h_l^2\gamma_m$, where γ_m is the unit weight of magma (Voight, 1974). In addition to the hydrostatically generated pressures from the magma column, magma 'overpressure' may exist to drive conduit flow (Rubin & Pollard, 1987). Such magma

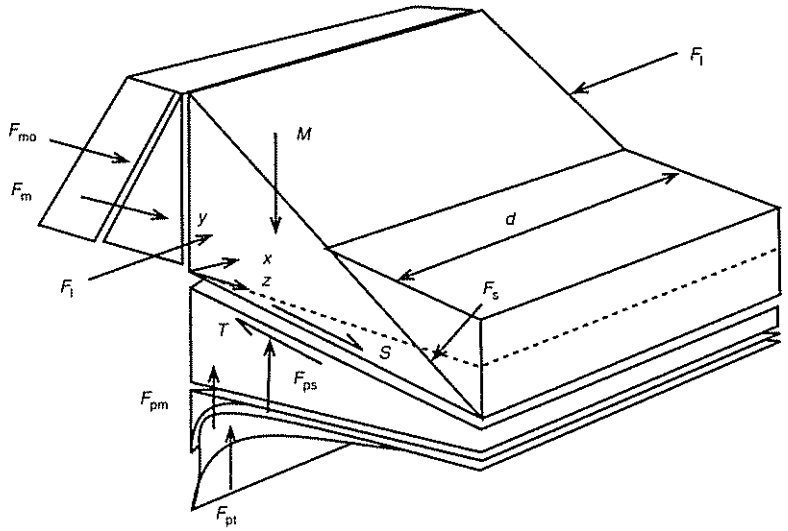

Fig. 8. Block geometry illustrating forces including lateral forces F_l and block width d. The influence of side restraint in resisting failure is evaluated in terms of effective stresses. The proposed fluid pressure distribution is integrated over the triangular face of the block and subtracted from the integrated total stress. All lengths are as defined in Appendix 1

overpressures generate an additional lateral force F_{mo}, for simplicity assumed constant with depth, defined as $F_{mo} = h_m p_o$, or $F_{mo} = h_m h_o \gamma_m$, where p_o is the magma overpressure and h_o is the 'equivalent excess height' of the magma column corresponding to the overpressure magnitude. The resulting lateral force F_m is defined as the sum of the two components, i.e. $F_m = \zeta(F_{ms} + F_{mo})$ as $\zeta = 1/2$ where the magma loading is applied over half of the rear block scarp for the mechanically induced pore pressures (Fig. 4) and over the full block width for thermally induced pore pressures as $\zeta = 1$.

Pore fluid pressures mechanically induced along the base of the wedge by the dyke intrusion process are given by equation (6). For this case, F_{pm} is a maximum when the leading edge of the dyke is in the centre of the slide block, and thus F_m is applied to half the block. Thermal pore pressure magnitudes are defined in equation (12). This idealization also approximates the potential influence of pore fluid processes induced by retrograde boiling, hydrothermal pressurization, or seismic shaking. Qualitative approaches for these conditions are also considered below.

Stability analysis

Resolving forces parallel to the basal failure plane in Fig. 7 enables the total force driving outward wedge movement to be determined as S. This force is opposed by the resisting shear force mobilized along the basal failure plane and lateral boundaries of the wedge. The width of the failure block is d. For simplicity, the mobilized shear force T is defined purely in terms of the 'apparent' frictional resistance ϕ, as

$$T = \frac{N \tan \phi}{F} \tag{15}$$

where F is the factor of safety against failure and N is the effective force normal to the failure surface. At failure, the components of the outward disturbing force S and the mobilized shear force T are, by definition, equivalent. Thus, setting the ratio T/S to unity enables the factor of safety for the slope to be defined as

$$\frac{F}{\tan \phi} = \frac{N}{S} \tag{16}$$

where the normal, N, and shear, S, components acting on the basal plane, and on the sides of the failing wedge, can be resolved from Figs 7 and 8 (for simplicity, the same frictional angle ϕ is assigned to basal and lateral failure planes). Resolving the components normal and parallel to the failure plane, and resubstitution into equation (16), gives

$$\frac{F}{\tan \phi} = \frac{\bar{M} \cos \alpha + \bar{F}_m \sin \alpha + \bar{F}_s \cos(\beta + \alpha) - \bar{F}_{pm} - \bar{F}_{pt} - \bar{F}_{ps} + \bar{F}_l}{-\bar{M} \sin \alpha + \bar{F}_m \cos \alpha - \bar{F}_s \sin(\beta + \alpha)} \tag{17}$$

where the overbar denotes the non-dimensional

magnitude of the forces. Forces acting on the wedge are made dimensionless by dividing throughout by $\gamma_w h_s^3$. M is the weight of the failing block, F_m is the composite lateral force generated by the combined magma column pressure and magma overpressure, F_s is the 'downward' force on the wedge resulting from loading by seawater, F_{pm} is the uplift force for pore fluid pressures mechanically generated by dyke intrusion, F_{pt} is the uplift force supplied by the thermal or hydrothermal mechanisms or by pressurized volatiles released from high-level magma chambers, F_{ps} is the force resulting from the static groundwater pressure and F_l is the lateral (side) force due to the effective lithostatic pressure. This lateral force is defined in terms of K_0, the coefficient of earth pressure at rest, given by the ratio of horizontal to vertical effective stresses (Lambe & Whitman, 1979). The distribution of solid body and pore fluid forces acting the failing block is defined in Fig. 8 and summarized in Appendix 1. For the subaerial case h_s is measured to the toe of the wedge, and F_s due to seawater is zero.

The peak-induced pore fluid pressure is truncated where it locally exceeds lithostatic stress. This pressure control implies the behaviour of a flexible, rather than rigid, sliding mass.

Controls on stability

From equation (17), the minimum set of dimensionless coefficients that describe the stability of the isothermal system may be determined as

$$\frac{F}{\tan\phi} = f\left(\alpha, \beta, \theta, \frac{\gamma_m}{\gamma_w}, \frac{\gamma_r}{\gamma_w}, \frac{h_m}{h_s}, \frac{d}{h_s}, \frac{h_o}{h_s}, K_o, w_D, \frac{Uh_s}{2c}\right) \quad (18)$$

In determining $F/\tan\phi$, the inclination of the basal plane α could be optimized to determine the critical magnitude α_c that defines the minimum factor of safety F for homogeneous materials. However, stratigraphy and structure control the distribution of strength, and hence selected inclinations of the failure plane that are compatible with the volcano structure and stratigraphy should be used to evaluate stability. An upper bound results, since failure modes that seem kinematically more critical are excluded by the overriding influence of weak layers.

Additionally, the parameters β, ϕ, γ_m/γ_w, γ_r/γ_w and K_0 are commonly constrained by relatively well-defined limits for many examples and may usually be estimated with some confidence. Eight primary variables remain that control behaviour. Two represent the variable geometry of failure through h_m/h_s and d/h_s, to define the depth and width of the failure plane respectively. The mechanical influence of the dyke is represented through the dimensionless dyke width w_D and the dimensionless dyke propagation rate U_D. Where thermal effects are included, the system is additionally controlled by the dimensionless groupings of parameters

$$\frac{AK_bD}{\gamma_w h_s}, \quad \frac{\kappa n}{c}, \quad \frac{4\kappa t}{h_s^2} \quad (19)$$

representing the magnitude of the thermal forcing A_D, ratio of thermal and hydraulic diffusivities D, and time t_D, respectively. Finally, where the influence of magma overpressure is added to the system, the additional variable representing excess magma column height, $h_o = h_s$, must also be accommodated.

Flank slip runout

The above analysis describes only the potential to initiate failure, and not the ability of the system to sustain failure, as required for long runout. Sustainable failure requires that the ratio of stabilizing to disturbing forces remain less than unity following initial failure. The components of forces driving flank failure are represented in the denominators of equation (17). The influence of slide weight M and forces due to sea level F_s does not change substantially under limited movement of the block. However, the driving influence of magma pressure will dissipate with displacement of the wedge.

The key components are the forces that act directly on the shear resistance ϕ of the basal and lateral failure planes. One influential factor involves the concept of residual strength; the residual or large-strain strengths for both indurated and non-indurated rocks are lower than the peak strengths mobilized at failure. Thus, once failure is initiated, strength drop occurs; under favourable conditions this drop may be sufficient to sustain failure in displacement-weakening materials. This generally implies that pore pressures are also not critically reduced as a result of failure and the consequent reorientation of stresses about the rupture plane, and indeed several viable mechanisms exist to raise or to maintain fluid pressures, as follows.

(*a*) Pore pressure response Δp may be quantified in terms of stress changes where the stress tensor is decomposed into independent components that represent changes in the 'mean' stress $\Delta\sigma_3$ and 'deviatoric' stress $\Delta\sigma_1 - \Delta\sigma_3$. The Skempton pore pressure relation (Skempton, 1954) defines such pore-pressure changes in terms of the pore-pressure coefficients A and B as $\Delta p = B\Delta\sigma_3 + A(\Delta\sigma_1 -$

$\Delta\sigma_3$). In particular, granular materials and clays with a loose, unstable structure may yield at failure a pore pressure in excess of the applied 'deviatoric' stress, i.e. $A > 1$. Altered tephra may also exhibit this characteristic (Anma, Maikuma, Yoshimura, Fujita & Okusa, 1988; Voight & Sousa, 1994). In dense granular materials and fractured rocks, local dilation that accompanies rupture may yield negative magnitudes of the pore pressure parameter (Goodman & Ohnishi, 1973); this would tend to arrest failure. The A parameter is not a constant material property, but depends on state of stress, stress history, total strain, and other factors. For sensitive materials and $A > 1$, the overriding outcomes of the process are a reduction in mobilized strength, an increase in pore pressure, and a corresponding reduction in mobilized restoring force.

(*b*) Pore pressure enhancement may occur as a consequence of frictional heat released during shear rupture propagation and basal slip (Voight & Faust, 1982, 1992). The process tends to reduce resistance to sliding and to sustain failure.

(*c*) Seismic shaking can cause pore fluid pressure enhancement, involving 'liquefaction' or 'cyclic mobility'. Under appropriate conditions, these pore pressures dissipate only slowly, and failure is sustained.

(*d*) For oceanic volcanoes, the sudden undrained loading of the 'unstable' marine sediments surmounted by the toe of the displacing volcano flank is likely to result in a profound drop in slide shear resistance. With further displacement of the flank, progressively more of the basal shear resistance of the displacing block is borne on these weak sediments, and an accelerating instability may result. Acceleration implies that resisting forces remain less than driving forces. As speed increases, submarine hydrodynamic drag augments the resisting force and places limits on acceleration, velocity and runout.

(*e*) For subaerial slides, rapid undrained loading of saturated alluvium and slide debris may provide similar mechanisms of fluid pressure generation (Hutchinson & Bhandari, 1971; Hutchinson, 1986; Sassa, 1988; Voight & Sousa, 1994).

(*f*) Friction-reducing fluid pressures may develop as a consequence of the transformation from simple basal sliding to bulk flow of debris.

These mechanisms are not quantified in detail here, but it is observed that under appropriate conditions they may be sufficient to sustain failure. Therefore large runout, post-failure displacements are not regarded as enigmatic, and prodigious, long runout terrestrial or submarine landslides are not unexpected provided volcano collapse is vigorously initiated.

COLLAPSE OF OCEANIC VOLCANOES

Collapses have been recorded for many oceanic volcanoes. Seventeen gigantic volcanic mass movements have been identified from Kauai to Hawaii, as summarized in Moore *et al.* (1989), and about 40 more have been found along the Emperor Seamount Chain from Kure Island to Kauai (Holcomb & Searle, 1993). Similar phenomena are known from the Indian Ocean at Réunion Island (Duffield, Stieltjes & Varet, 1982; Lénat, Vincent & Bachelery, 1989; Labazuy & Lénat, 1990), and at Tristan da Cunha and the Canary Islands in the Atlantic (Holcomb & Searle, 1993). Arcuate margined atolls, often with corresponding bulging submarine contours, probably also reflect submarine volcano collapses and are reported from the Central Pacific in the Makin, Kuria, Aranuka, Gilberts, Carolines, and Marshalls, as well as from stratovolcanoes in the Banda Sea (Fairbridge, 1950).

Both relatively shallow and deep-seated failures have been recognized in the submarine surveys. Deep-seated 'slump' failures comprise a deep basal failure plane, relatively flat and sometimes dipping in the opposite direction to the overlying flank. Such failures may cause rapid but limited displacement and may augment the earthquake record but, due to the geometry of the basal plane, are incapable of sustaining long runout.

The shallow failure model, emphasized in this paper, is characterized by a failure plane sloping in the same direction as the volcano flank and can produce the rapid, long runout 'debris avalanches' evident in the bathymetric record (Moore *et al.*, 1989). The term 'shallow' is used here in a relative sense, in comparison with the dimensions of the volcano edifice. Such shallow slides may indeed produce prodigious mass movements, involving volumes as great as 5000 km^3 and reaching more than 200 km from their source.

Typical oceanic volcanic structure is shown in Fig. 9. A basal prism of submarine pillow basalt and intrusives is covered by a mantle of glassy clastic debris and subaerial basalt flows (Hill & Zucca, 1987). The enveloping geometry for analyses presented here is a flank rising at an angle β of 10° from the sea floor with the static groundwater surface rising from sea level at an angle θ of 2°. Material parameters are given in Table 2. Some estimates of frictional resistance ϕ are provided in Table 2, but as the results of the analyses are reported through the normalized quantity $F/\tan\phi$, the results are not constrained by the estimates provided. At the initiation of

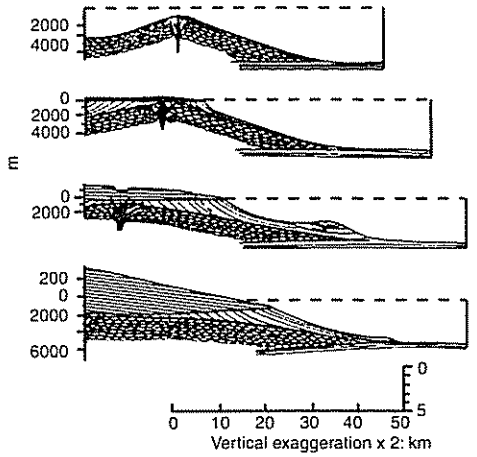

Fig. 9. Cross-sections illustrating oceanic volcanic islands in submarine, sea-level and subaerial stages of evolution (reproduced from Moore & Fiske, 1969). Patterns indicate rock types: ovals, pillow lavas with included pillow fragments and sediment; lined pattern, clastic rocks, including phreatic-explosion ash, littoral-cone ash and flow-foot breccia and some pillowed flows and pillowed breccias; dark pattern, subaerial lava flows with minor ash; solid black, intrusive rock. Note contrast between submarine and subaerial slopes, continuation of clastic layer beneath subaerial shield, and downbowing of sea floor by subsidence caused by volcanic loading. Dyke swarms may occur deep within the edifice, overprinted on pillow lavas

failure, $F \rightarrow 1$ and values of $F/\tan\phi$ are of the order of 1·9 to 1·2 for friction angles ϕ of 28° and 40° respectively.

Basic modelling considerations

For shallow flank failure in the absence of induced pore pressure change but in the presence of a magmastatic force F_m, stability is conditioned only by lateral restraint, width of the failing block, and depth and angle of the basal failure plane. All other parameters are constrained by the assumed geometry, and the narrow ranges of the density parameters, defined in Tables 2 and 3. The geometry of the system constrains the dip of the failure surface to less than the surface slopes; for uniform materials a critical inclination of $\alpha_c = 6°$ is evaluated for large dimensionless widths $d_D = d/h_s$. Using this failure plane inclination, stability is evaluated for different magnitudes of lateral earth pressure coefficient K_0 and depth of failure h_m/h_s (Fig. 10). Where the effects of lateral restraint are discounted ($K_0 \rightarrow 0$), it is apparent that very shallow failure (say $h_m/h_s = 1$) is easiest to initiate due to the diminished influence of the stabilizing force due to loading by seawater F_s. At increasing

Table 2. Material parameters selected as representative of mechanical and thermal properties of volcano flanks

Parameter (reference*)	Magnitude
Slope height above sea level h_s	1000 m
Shear modulus G (1)	3×10^3 MPa
Poisson ratio ν (2)	0·22–0·28
Frictional resistance ϕ†	20°–60°
Coefficient of earth pressure at rest K_0 (3)	0·5
Unit weights	
Water γ_w	10×10^{-3} MPa/m
Rock γ_r (4)	$23–29 \times 10^{-3}$ MPa/m
Magma γ_m (5)	$26–28 \times 10^{-3}$ MPa/m
Volcaniclastic debris†	
Permeability k/μ (6)	$1–2 \times 10^{-11}$ m²/Pa.s
Hydraulic diffusivity c (6)	770–1550 m²/s
Intrusion width w (7)	1 (1×10^{-3})§ m
Intrusion rate U (8)	0·27–0·75 m/s
Fractured lava‡	
Permeability k/μ (9)	$1·65–7·2 \times 10^{-6}$ m²/Pa.s
Hydraulic diffusivity c	$1·5–6·5 \times 10^6$¶ m²/s
Intrusion width w (10)	1 m
Intrusion rate U (11)	0·1–0·5 m/s
Thermal parameters	
Thermal strain A† (12)	0·9–1
Skeletal modulus K_b (12)	$0·4–1·2 \times 10^3$ MPa
Thermal diffusivity κ (12)	10^{-6} m²/s
Porosity n (12)	0·05–0·2

* References: 1, Davis cited by Rubin & Pollard (1987); 2, Rubin & Pollard (1987); 3, estimated from Dieterich (1988); 4, Zucca & Hill (1980), Zucca, Hill & Kovach (1982), Rubin & Pollard (1987); 5, Decker (1987); 6, Sigurdsson (1982); Bodvarsson, Benson, Sigurdsson, Stefansson & Eliasson (1984); 7, Tryggvason (1980), Elsworth & Voight (1992); 8, Brandsdottir & Einarsson (1979), Elsworth & Voight (1992); 9, Thomas (1987), Mink & Lau (1990); 10, Delaney & Pollard (1981), Rubin & Pollard (1987); 11, Delaney & Pollard (1981); 12, Delaney (1982).

† Possibly ϕ may be close to, or lower than, the lower limit of the range where clays dominate the key stratigraphic horizon. Lower range values are representative of clays and mudstones, including altered tephras. Upper range values are representative of angular granular debris or weak rock, and include the effect of cohesion on apparent friction angle.

‡ Volcaniclastic data are based on studies at Krafla volcano by authors cited; lava data are based on studies in the Hawaiian Islands by authors cited.

§ Unbracketed value represents observed thickness. Bracketed value represents thickness estimate consistent with parameters used in the evaluation of intrusion-induced fluid pressures. See discussion in text.

¶ Magnitude of hydraulic diffusivity is estimated from $c = 2(k/\mu)G(1-\nu)/(1-2\nu)$ to give representative value for incompressible fluid and grains (Rice & Cleary, 1976). Parameter range obtained using $\nu = 0·25$ and shear modulus G and permeability k/μ ranges given in the table.

Table 3. Dimensionless parameters used in evaluation of mechanically induced pore pressures

Dimensionless grouping*	Parameter range	Reference§
γ_m/γ_w	2·6	
γ_r/γ_w	2·3	
Volcaniclastic debris		
w_D†	2·5–30 × 10^2	1
	0·25–4 × 10^6	2
U_D‡	0·1–1	
Fractured lava		
w_D^*†	1–1 × 10^{-3}	
U_D^*‡	0·4–1·7 × 10^{-4}	

* Dimensionless parameters of width w_D and intrusion velocity U_D are defined in equations (6) and (3) respectively.

† Magnitude of w_D is estimated from the material coefficients and geometric parameters of Table 2. The upper bound magnitude is representative of a 1 m wide dyke, and the lower bound is for a 10^{-3} m wide dyke consistent with the parameter evaluations of Elsworth & Voight (1992).

‡ Estimate uses permeability and hydraulic diffusivity parameters for the two volcanic environments, with other data from Table 2. An intrusion velocity of 0·5 m/s is considered representative of both Icelandic and Hawaiian eruptions.

§ References: 1, Elsworth & Voight (1992); 2, Tryggvason (1980) and Delaney & Pollard (1981).

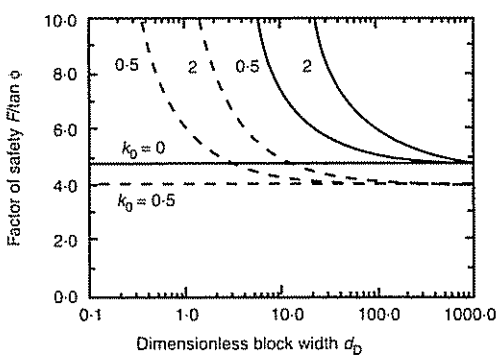

Fig. 10. Normalized factor of safety for failure of an oceanic volcano flank in the initial condition with static groundwater conditions. Results are for the critical failure plane inclination of $\alpha_c = -6°$ and for contrasting failure heights h_m/h_s of 1 (dashed) and 10 (solid). Variable values of coefficient of earth pressure at rest K_0

depth this stabilizing influence increases faster than the buildup in driving force from the magma.

The influence of lateral restraint decreases as dimensionless block width $d_D = d/h_s$ increases. For an increasing depth of failure, an increased failure width is necessary to enable the problem to be approximated by two-dimensional rather than three-dimensional form. For $h_m/h_s = 10$ the required width becomes prohibitive, even for relatively modest values of K_0 (Fig. 10). For shallower systems ($h_m/h_s = 1$), the value of K_0 is less critical (Fig. 10). In the environment characteristic of volcanoes, sub-lithostatic magnitudes of lateral stresses are generally expected (Rubin & Pollard, 1987; Dieterich, 1988); $K_0 = 0·5$ is presumed reasonable. In the absence of an initiating mechanism, and with nominal values of frictional resistance ϕ, the representative wedge characterized by Fig. 10 is expected to remain stable.

Pore fluid pressures mechanically generated by intruding dyke

Where mechanically induced pore fluid pressures are added to the static behaviour, control is exerted by two additional parameters: dimensionless intrusion rate U_D and dimensionless dyke width w_D (see equations (3) and (7)). Field-test-based estimates of permeability and hydraulic diffusivity are provided for two representative materials: compact, partly altered basaltic volcaniclastic debris, and fractured, weathered basaltic lava (Table 2). For the slope geometry of Hawaii, dimensionless intrusion rates U_D are in the range 10^{-4}–10^0.

The dimensionless rate of intrusion influences the morphology of the pressure bulb that develops around the advancing dyke front (Elsworth, 1991). As U_D increases to and beyond 10^0, the pressure bulb becomes elongated along the path of propagation (x-axis; see Fig. 5). For $U_D > 10^0$ the resulting pressure bulb is no longer elongate but exhibits a circular section in the x–z plane. As the intrusion rates anticipated for this system straddle the boundary between these two different forms of behaviour, both effects are manifest in the stability response. With regard to stability, the relevance of this observation is that $U_D > 10^0$ results in induced pressures more tightly constrained close to the dyke location. Slower propagation results in a more widespread distribution of pore fluid pressures over the failure plane, and although of lower absolute pressure magnitude, the influence exerted on stability is more widespread.

Whereas dyke propagation rate primarily influences the distribution of induced pore pressures, dyke width, through w_D, controls the absolute magnitude of induced pressures. In the original matching of induced pressures observed at Krafla volcano with the model presented in equation (1), a low estimate was returned for dyke width. This discrepancy occurred despite satisfactory evaluation of other parameters of propagation rate U and dyke location. Where the same techniques are used to characterize the form of hydrofractures created in the stimulation of petroleum reservoirs, a similar

underestimation of the fracture volume results (Elsworth & Piggott, 1992). The disagreement between the 'evaluated' volume and 'real' volume apparently results from the influence of the free surface that is not accounted for in the solution for a dislocation in an infinite medium (Ouyang, 1994). The effect of the free surface, to dampen the magnitude of the induced pore pressure response, becomes more acute as the dyke approaches the free surface, as was the case for Krafla. The dichotomy may be resolved by using a range of parametrically consistent values of material parameters. Thus values in the range $10^{-1} \leqslant U_D \leqslant 10^0$ and $10^2 \leqslant w_D \leqslant 10^6$ are selected for volcaniclastic material, and $U_D = 10^{-4}$ and $10^{-3} \leqslant w_D \leqslant 10^0$ are selected for rock-mass lava, to compare trends in behaviour (Table 3).

Figures 11(a) and 11(b) represent behaviour consistent with failure in volcaniclastic materials. For the upper bound of $U_D = 10^0$, as represented in Fig. 11(a), a variety of trends are apparent. For very small dyke widths ($w_d \leqslant 10^{-1}$) there is no influence of mechanically induced pore fluid pressures and the trend in decreased stability with increased width follows directly. As dyke width is increased above 10^1, the influence of mechanically induced pore fluid pressures monotonically increases. For narrow blocks, the stabilizing effect of lateral restraint dominates behaviour. For intermediate magnitudes of dyke width, say $w_D = 10^4$, the stability curve exhibits three distinct zones, separated by cusps. The first zone is for dimensionless block width $d_D \leqslant 10^1$ and illustrates the rapidly diminishing influence of lateral restraint with increased block width. For this large magnitude of U_D the induced pressure distribution is elongate and the mechanically induced uplift force F_{pm} increases in direct proportion to width. Thus for small block widths, $d_D < 10^1$, the pressure distribution is effectively identical in all parallel sections in the y–z plane (the plane of cross-section; see Fig. 4) but for a second zone delimited by $10^1 \leqslant d_D \leqslant 2 \times 10^2$, an increase in stability occurs gradually with increased block width. This rate of gain in stability is reduced as the block width approaches the upper limit of its range. In this zone the uplift force increases less quickly than block width as the ends of the elongate pressure distribution are felt inside the expanding area of the failure surface. This is especially pronounced for $U_D > 10^0$, where the centre of the pressure distribution lags behind the advancing dyke front (Elsworth, 1991). Thus, the uplift force increases at about half the rate of increase in dimensionless block width d_D as the true three-dimensional nature of the distribution becomes apparent between the limits of integration. The third zone is for $d_D \geqslant 2 \times 10^2$ and represents constant uplift force F_{pm} as width increases. At these block widths the pressure pulse is entirely contained within the lateral extent of the failure plane and its relative influence diminishes as $d_D \rightarrow \infty$.

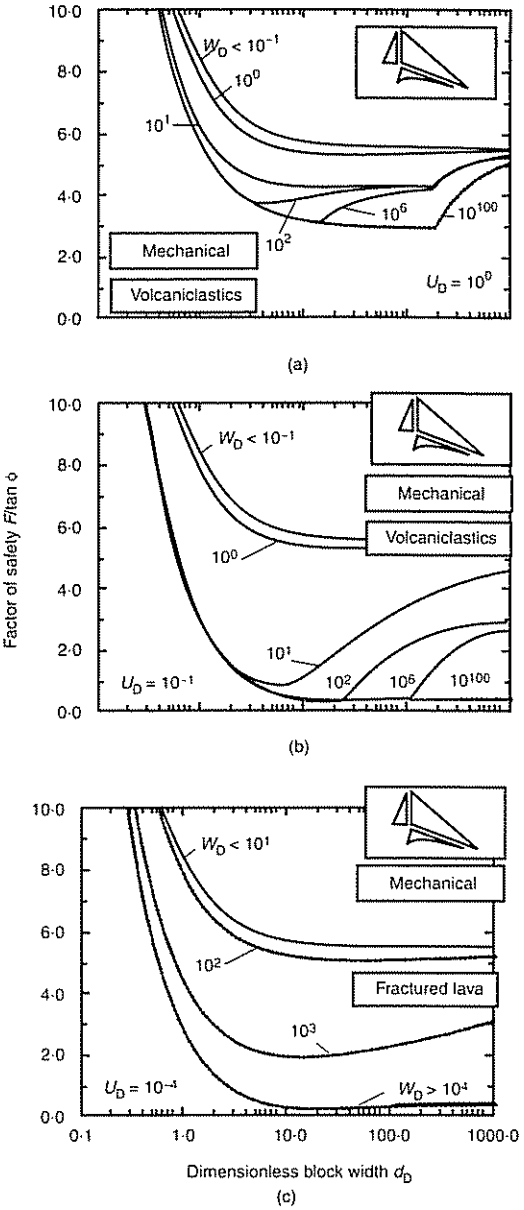

Fig. 11. Normalized factor of safety for failure of an oceanic volcano flank with mechanically induced pore pressures resulting from dyke intrusion. Basal failure plane is inclined at $\alpha = -6°$. $h_m/h_s = 1$. For volcaniclastic materials: (a) $U_D = 10^0$; (b) $U_D = 10^{-1}$. For fractured lava: (c) $U_D = 10^{-4}$. The observed range of dimensionless dyke widths are shown (solid), as are those larger than observed (dotted)

The presence of a minimum stability for w_D in the range 10^2 to 10^6 is important. For values of $F/\tan\phi$ approaching 2 the slopes may be approaching the initiation of failure (i.e. for $\phi = 27°$, then $\tan\phi \approx 0{\cdot}5$ and $F/\tan\phi \approx 2$, consequently $F = 2 \times 0{\cdot}5 \approx 1$; and by definition, at failure, $F = 1$). The range of failure widths at these minima are d_D of the order 2–10, representing block width $d = 2$–10 km for the selected geometry with $h_s = 1$ km.

As dimensionless dyke propagation rate is decreased to $U_D = 10^{-1}$, representing a propagation rate of 10^{-1} m/s (if hydraulic diffusivity is held constant), the stability of the system is substantially reduced even for moderate values of dyke width (Fig. 11(b)). Similar trends in behaviour are evident as for the 'faster' intrusion, although minimum factors of safety are diminished. Thus mechanically induced pore pressures appear theoretically sufficient to trigger failure to block widths of as much as 100 km.

For material parameters possibly representative of fractured basaltic lava (Fig. 11(c)), the influence of mechanically induced pore fluid pressures appears insignificant. Thus for this mechanism, failure in volcaniclastic materials appears plausible, but failure in fractured lavas does not.

In addition to magmastatic disturbing forces, additional magma overpressurization of the order of 10 MPa may sometimes occur (Rubin & Pollard, 1987), and may reduce the stability of flanks. A comparison of Fig. 12 with Figs 11(a) and 11(b) illustrates the potentially important influence of magma overpressurization on stability.

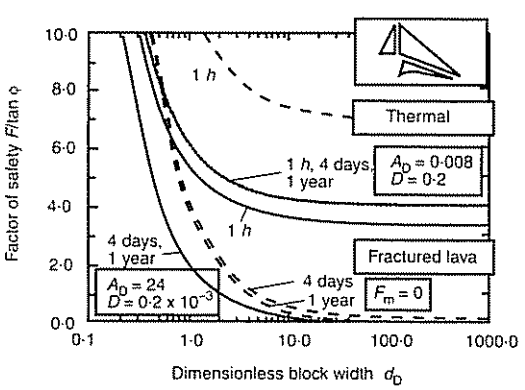

Fig. 12. Normalized factor of safety for failure of an oceanic volcano flank with thermally-induced pore pressures resulting from intrusion. Comparison of minimum (dotted) and maximum (solid) thermal forcing parameters. Analysis includes magmastatic forces. Basal failure plane is inclined at $\alpha = -6°$. Also included is the behaviour where the magma driving force is removed (dashed) following the initiation of block movement

Pore fluid pressures thermally generated by an intrusion

Thermal strains and thermally driven groundwater flow may generate and spread additional excess fluid pressures. Although dyke-generated mechanical and thermal mechanisms are additive, the occurrence of maximum influence from each mechanism is unlikely to coincide in time. Thus, the thermal influence is examined in isolation.

Using the thermal parameters defined in Table 2, the appropriate ranges for the dimensionless parameters of thermal forcing A_D, diffusivity ratios D and time t_D are determined (Table 4). The magnitude of thermal strain A^* resulting from a prescribed temperature boundary condition is relatively insensitive to the choice of depth or thermal rise magnitude (Delaney, 1982; Table 4). The parameter with the widest natural variability in the constants A_D and D remains the ratio of thermal to hydraulic diffusivities D, representing a material property rather than the magnitude of the thermal forcing. The time-scale of interest includes representative values of 1 h, 4 days and approximately 1 year (400 days).

For the parametric groupings representing the least destabilizing thermal effect, the influence on stability is barely discernible (Fig. 12). Conversely, the selection of maximum thermal forcing has a profound influence on stability. For this choice of parameters, the thermally induced pore pressures are sufficient to induce failure in time periods over several days to months. This model requires that the continuous temperature boundary condition at the dyke face is maintained by a replenished supply of fresh magma over periods of this same order. This condition may be roughly consistent with a feeder dyke, but not with a 'blind' dyke that fails to reach the surface, or one that is active only for a brief period. The sustained discharge of water in 1973 observed from a deep drillhole about 2 km from an erupting fissure at Heimaey, Iceland,

Table 4. Dimensionless parameters used in evaluation of thermally induced pore pressures

Dimensionless grouping	Parameter range
A_D^*	24–0·008
D	$0{\cdot}2 \times 10^{-3}$–200×10^{-3}
t_D	0·014, 1·4, 144 $\times 10^{-6}$†

* The broad parameter range of A_D is conditioned mainly by the variability of hydraulic diffusivity, as represented in the ratio of thermal and hydraulic diffusivities D. Change in thermal forcing anticipated at depth is reflected through the parameter $A^* = \alpha\Delta T$ (see equation (9) and Table 2) which remains relatively insensitive to the magnitude of temperature increase.

† Dimensionless times represent dimensional times of 1 h, 4 days and 400 days.

probably reflects this mechanism augmented by volatile heat transfer (Björnsson *et al.*, 1977). Under such conditions, thermal straining of the host rock appears a viable agent to raise pore pressures in confined aquifers, and to initiate flank failure in zones of weak materials.

Following failure, the ensuing small displacements may result in a significant decrease in the magmatic driving forces acting on the wedge. Unless the induced basal pore pressures are sufficiently large to maintain the instability, failure will arrest. A limiting case for flank stability is illustrated in Fig. 12, where the driving magma force is removed; here the factor of safety relates to the period after the initiation of movement, and its low value illustrates the potential of this mechanism to sustain motion.

Retrograde boiling, hydrothermal processes and earthquake-induced strength loss

Results for thermal forcing are roughly similar to those obtainable for a constant pressure aquifer boundary and diffusive pressurization, associated with pressurized volatiles released by retrograde boiling of high level magma chambers. In the most extreme case, volatile injection may occur along weak strata interfaces, providing a film of virtually zero strength. Thus under appropriate conditions, retrograde boiling appears to be a viable agent to initiate flank failure in zones of weak, permeable materials.

Similarly, hydrothermal systems or earthquake shaking may induce profound strength loss, and in the limiting case the induced pore pressures can fully match overburden lithostatic stress. In certain cases, discrete water films can develop, with virtually zero strength.

The mechanical situation for these extreme but nevertheless plausible cases approaches that shown for maximum thermal loading in Fig. 12. Failure is again controlled by edge loading, thus block widths $d_D > 1$ can be generally expected, even where basal surface strength vanishes.

The destabilizing effect that results from the combined influence of magmatically or seismically induced pore fluid pressures may be determined by considering the effective time-scales of these processes. Pore pressures mechanically induced by dyke propagation are typically short-lived, and may be expected to be important over periods of hours to days. Thermal effects take longer to establish, and for the geometry considered in these examples, time-scales of weeks to months appear more appropriate. Thus the effects of these two components are not necessarily additive, but are better considered as separate mechanisms. However, seismic-induced pore pressures may be produced over broad areas in minutes, but in some cases may have a duration of months, depending on the materials and boundary conditions. The case of retrograde boiling is generally comparable to thermal loading unless hydrofracture sill (horizontal injection) propagation follows potential sliding surfaces, in which case the loading may be nearly instantaneous. Consideration of separate mechanisms leaves the resulting stability analysis as a conservative evaluation.

Seismic influence on driving forces

The capability to develop earthquakes of significant magnitude is a natural consequence of magmatic intrusion, potentially involving both magmatic driving force source mechanisms and pore fluid pressurization mechanisms. Where pore fluid pressurization mechanisms are activated, the resulting seismic energy release may be much larger than that potentially released for the similar case with magmatic driving forces, but lacking pore pressure enhancement (Voight & Faust, 1979). The effects of seismicity induced in this manner, or from regional tectonic earthquakes, are manifest in the potential reduction in shear resistance in adjacent materials subject to porosity change and liquefaction, and also through the destabilizing influence of strong motions. Earthquake forces are clearly capable of augmenting the load driving a potential slide mass (Pariseau & Voight, 1979; Keefer, 1984; Hutchinson, 1987). Quantitative evaluations of stability include analyses requiring detailed time history of acceleration records and properties of materials (typically non-linear and hysteretic) under dynamic loading (cf. Newmark, 1965; Ambraseys & Sarma, 1967; Seed, Lee & Idriss, 1969; Seed, 1981). The alternative and standard procedure is the pseudostatic method (Taylor, 1948; Terzaghi, 1950; Seed, 1979), which despite some limitations offers a simple and often adequate means to evaluate the sensitivity of slope behaviour to seismic loading. This latter procedure has been used for stability analyses at Mount St Helens volcano (Voight *et al.*, 1983) and is also used here.

The stability of shallow failures is examined for slopes subjected to a uniformly distributed effective lateral acceleration δ of the order of 0·1 g to 0·2 g, acceleration magnitudes consistent with sizeable earthquakes characteristic of volcanoes. The 1975 Kalapana earthquake (M_s7·2) and the 1983 Kaoiki (M_s6·6) earthquake are typical of Hawaiian events of sufficient size to cause structural damage and to influence the stability of shallow slopes (Tilling, Koyanagi, Lipman, Lockwood, Moore & Swanson, 1976; Buchanan-Banks, 1987; Ando, 1979).

The influence of lateral acceleration on stability is judged from its pseudostatic influence on the

limit equilibrium relation of equation (17). The components of the lateral acceleration are resolved perpendicular and parallel to the failure surface. Correspondingly, the numerator term of equation (17) is transformed as $\bar{M}\cos\alpha \rightarrow \bar{M}(\cos\alpha + \delta\sin\alpha)$ and the denominator as $-\bar{M}\sin\alpha \rightarrow -\bar{M}(\sin\alpha - \delta\cos\alpha)$. The pseudostatic effect increases the outward destabilizing force while simultaneously affecting the shear resistance on the failure surface. For failure on an outward-dipping slide surface these processes act additively to reduce the factor of safety.

Pseudostatic accelerations of 0·1 g or 0·2 g are applied to the conventional geometry with static groundwater pressures and magmastatic pressures on the rear scarp (Fig. 13). Stability is reduced with increased acceleration, especially for blocks with relatively large width where the influence of side restraint is less pronounced. Where the 0·1 g acceleration is superimposed on an already profound thermal fluid pressure effect, the potential for failure becomes apparent, even after relatively small periods of exposure to heating (hours to days). A similar result may be anticipated for pore pressures significantly enhanced by seismic vibration, or for pore pressure rise reflecting pressured volatile release from magma chambers.

In some cases the effects of magmatic intrusion on landsliding can be complex and indirect. Thus the Hilina fault system in Hawaii (cf. Stearns & MacDonald, 1946; Moore & Krivoy, 1964) may be interpreted as the headwall of a large gravity slump episodically destabilized by seismic ground motion; in this case the earthquakes may be caused by forceful magma intrusion in deeper parts of the volcano, and consequently the slump is regarded as a secondary surficial feature only indirectly related to magmatic processes.

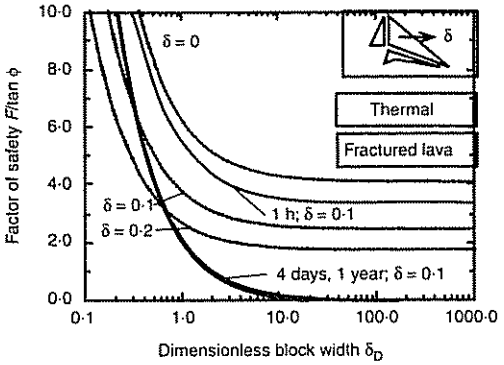

Fig. 13. Normalized factor of safety for failure of an oceanic volcano flank subject to lateral pseudostatic earthquake acceleration δ and with only static groundwater (dotted) and thermally induced pore fluid pressures (solid) applied. Magmastatic pressures are applied for all analyses. Basal failure plane is inclined at $\alpha = -6°$ and $h_m/h_s = 1$

COLLAPSE OF COMPOSITE VOLCANOES

Historic eruptions of composite volcanoes associated with major slope failures include those with a magmatic component (Bezymianny type) and those solely phreatic (Bandai type) (Siebert *et al.*, 1987), following previous designations of Gorshkov (1962) and Moriya (1980).

At Bandai in 1888, failure of the north flank resulted in a 1·5 km^3 debris avalanche which buried an area of 34 km^2 with several villages, and blocked river drainages to form five new lakes (Fig. 14; Sekiya & Kikuchi, 1889). The slope failure probably occurred in a retrogressive sequence, with three main stages as indicated in Fig. 15(a) (Yonechi, 1987). The accompanying eruption included several low-angle explosions, but was

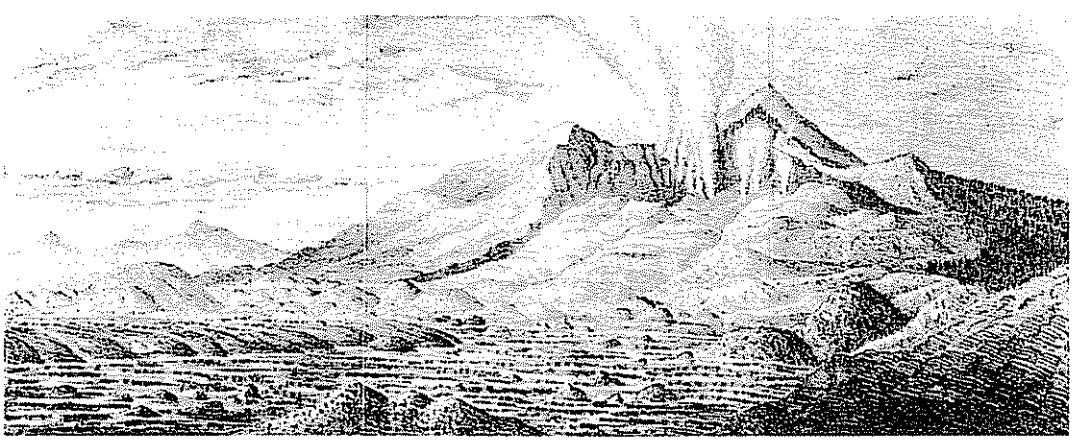

Fig. 14. Bandai volcano, Japan. Slope collapse 15 July, 1888. Lithograph from Sekiya & Kikuchi (1889) shows hummocky topography of avalanche deposit, with the debris partly filling the avalanche scar. Phreatic (steam) plumes near the rear scarp arise from the hydrothermal system of the volcano. No fresh magma had intruded into the upper cone

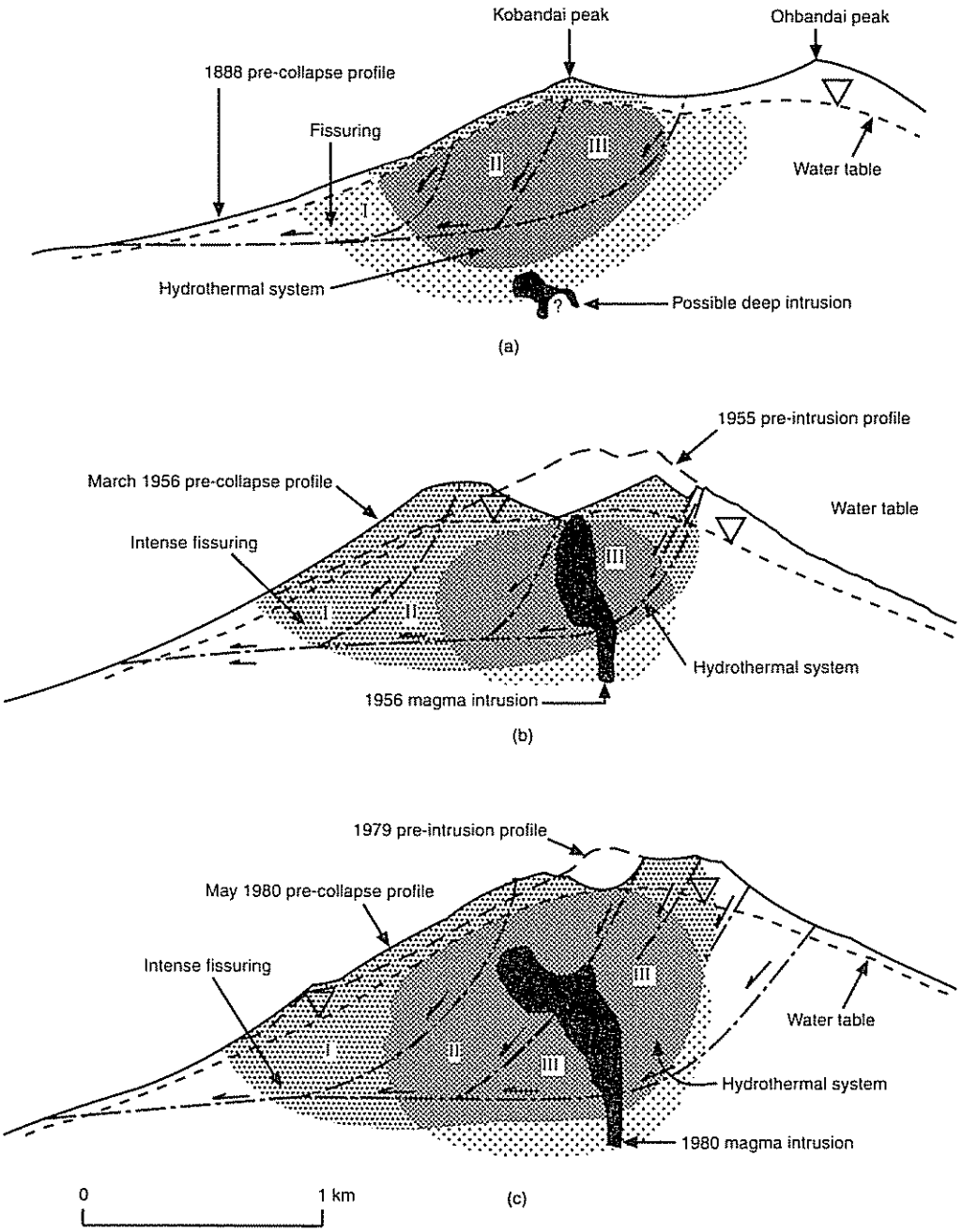

Fig. 15. Cross-sections of composite volcanoes associated with major slope collapse: (a) Bandai volcano, 1888; (b) Bezymianny volcano, 1956; (c) Mount St Helens volcano, 1980. Cross-sections show pre-intrusion and pre-collapse profiles, inferred water tables, and zones of intense fissuring, hydrothermal systems, and fresh magma intrusions. No intrusion was detected at Bandai, but those at Bezymianny and Mount St Helens caused large-scale deformation of the cone and steepening of the flank. In all three cases, collapse is interpreted as retrogressive failures of three principal blocks, the succession indicated by Roman numerals. In cases (b) and (c), intrusions were directly involved in the collapse. The great relative depths of the avalanche scars are attributed to the fragmental, highly fissured, or altered material in the core of the volcanoes, and to the fluidized nature of these materials in association with overpressured and explosive hydrothermal and magmatic systems

strictly phreatic because no fresh (juvenile) magma products have been found in either the debris avalanche or tephra deposits.

At Bezymianny, slope failure on 30 March 1956 was preceded by about a half year of magma intrusion and associated large-scale deformation of the volcano flank (Gorshkov, 1959). Eruptions of fresh andesite had begun in October 1955. The slope failure resulted in a 0·8 km^3 debris avalanche covering an area of 60 km^2 (Fig. 16). Associated low-angle explosions, with fresh magma products, devastated an area of 500 km^2. The authors believe that retrogressive slope failure preceded and initiated the lateral explosions at Bezymianny (Fig. 15(b)), much as at Mount St Helens in 1980 (Fig. 15(c)).

The events at Mount St Helens and at Bezymianny were similar in many respects, but the documentation of processes at Mount St Helens is unexcelled. At Mount St Helens, retrogressive failure in three main stages on 18 May 1980 was preceded by two months of magma intrusion and large-scale deformation of the north flank (Fig. 15(c); Voight *et al.*, 1983). The slope failure resulted in a 2·5 km^3 debris avalanche blanketing an area of 64 km^2 (Voight *et al.*, 1983, Sousa & Voight, 1991, 1995). Associated low-angle explosions containing fresh magmatic products devastated an area of about 600 km^2 (Siebert *et al.*, 1987).

Almost 200 cases of Quaternary large volcanic debris avalanches have been tabulated by Siebert *et al.* (1987). There is a broad spectrum of volcano slope failure modes, ranging from those without coeval eruptions to those that include laterally-directed explosions, and/or vertical eruption columns, of variable character and intensity. In this paper the terms Bezymianny and Bandai are used also to refer to the major slope failures on composite volcanoes accompanied by explosive eruptions. The implication is that for the former type (Fig. 15(b)) magma has intruded into the upper edifice and may directly influence stability; for the latter (Fig. 15(a)) magma apparently plays

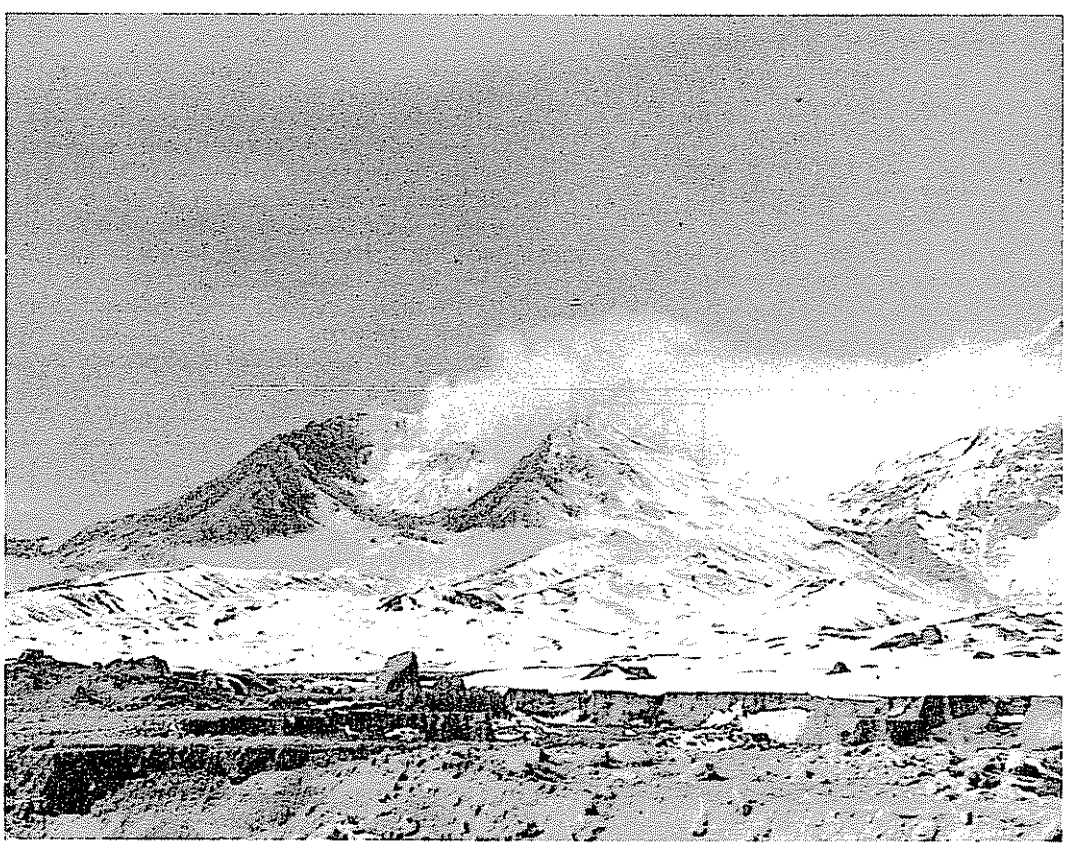

Fig. 16. Bezymianny volcano, Kamchatka. Slope collapse 30 March, 1956. This June 1956 photograph shows scattered avalanche debris in foreground. The avalanche scar is partly filled by an extrusive dome of viscous lava squeezed out after 30 March. Magma intrusion between October 1955 and March 1956 caused large-scale deformation of the cone, and was instrumental in the slope collapse

no direct role in the slope failure. If intrusions are indeed present in the latter instance, they are deeper within the edifice, and any relation to instability must be indirect or involve merely volatile separation. For both types, hydrothermal processes may play a role in stability in weakening the edifice materials, and in fluid overpressurization.

In this paper, stability models with applied magmatic forces simulate the Bezymianny-type collapse with upper edifice intrusions; analyses lacking such forces simulate Bandai-type failures, collapses that trigger eruption from deep-seated magma chambers, or mass movement types unaccompanied by eruptions.

The geometry chosen in most analyses is a flank rising at an angle β of 30°, a static groundwater surface rising from the toe of slope at $\theta = 18{\cdot}5°$, and a basal failure surface dipping outwards at $\alpha = -7°$.

Using these 'standard' values, stability is evaluated as a function of dimensionless block width d_D for magnitudes of lateral earth pressure coefficient $K_0 = 0$ and 0·5. Four cases of rear-scarp loading are used for a sensitivity evaluation, namely

(*a*) zero magma loading
(*b*) half-depth dyke penetration
(*c*) full-depth dyke penetration
(*d*) full-depth dyke penetration with overpressure (Fig. 15).

Both the normalized factor of safety and the relative influence of lateral restraint decrease as magma pressures increase (Fig. 17). For decreased magmatic involvement, an increased failure width is necessary to enable the problem to approach 'two-dimensional' factor of safety values for unrestrained plane failure as indicated by $K_0 = 0$. Failure may be feasible at nominal values of ϕ for a fully-penetrating magma intrusion, without any additional mechanism.

For modest values of K_0 the results suggest that block width should generally equal or exceed depth to the failure surface (e.g. $d_D > 1$). This result is consistent with field observations of volcano avalanche scars: of 106 data sets for 'composite' volcanoes reported by Siebert *et al.* (1987), only four reported widths were less than 1 km, and the minimum was 0·7 km. In addition, only 15 values exceeded 5 km, and of these only 3 exceeded 10 km; the maximum value was 14 km. The limits reflect typical composite cone geometry and size.

For the same four cases of rear scarp loading, stability is evaluated for a uniformly distributed effective lateral acceleration of $0{\cdot}1g$ (Fig. 18). The influence is to reduce stability, with the change being most dramatic for partial-penetration magma loading and for zero edge loading. For the former, failure may be feasible (assuming weak sliding materials) without additional mechanisms, for approximately $d_D > 3$. For the latter, more intense earthquake loading or supplementary fluid pressurization mechanisms (Table 1) are required for failure. It should be noted that different failure surface geometries, e.g. curved arc or active–passive wedge blocks, may exhibit lower factors of safety than those indicated for the simple triangular blocks in Fig. 18; also, joint-water forces applied to the rear scarp could reduce stability.

This result is qualitatively consistent with historical debris avalanches at Miyuyama, Bandai,

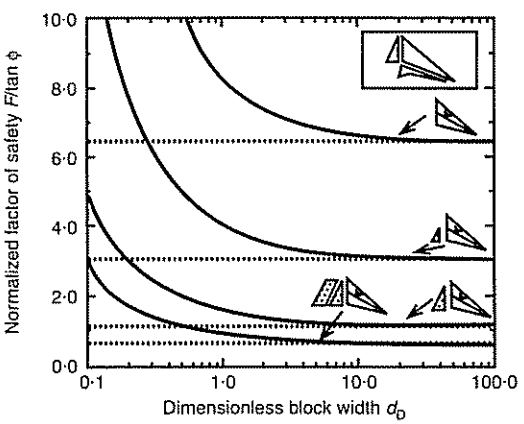

Fig. 17. Normalized factor of safety for failure of a composite volcano flank with static groundwater force $K_0 = 0$ (dotted) and 0·5 (solid) curves for zero magma loading, half-depth dyke penetration, full-depth dyke penetration, and full-depth dyke penetration with overpressure

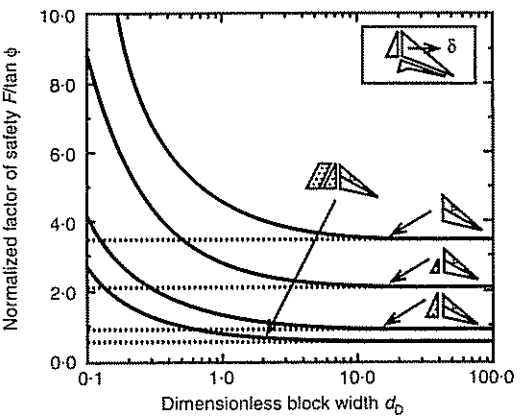

Fig. 18. Normalized factor of safety for failure of a composite volcano flank with static groundwater force and seismic loading $\delta = 0{\cdot}1$: magma loadings as in Fig. 17

Bezymianny, Shiveluch and Mount St Helens, all of which were accompanied by earthquakes with magnitudes of roughly $M = 5$ (Okada, 1983; Siebert *et al.*, 1987). The best documented cases are Mount St Helens and Bandai, where the evidence suggests that $M = 5$ earthquakes in fact triggered the instability (Voight *et al.*, 1981, 1983; Sekiya & Kikuchi, 1889; Okada, 1983).

It should also be noted that stability is markedly influenced by the piezometric conditions assumed. For example, raising the static piezometric surface to the ground surface makes the stability of the full-penetrating dyke case roughly comparable to the case for the overpressured dyke and 'standard' piezometric levels (cf. Figs 17 and 20).

Pore fluid pressures mechanically generated by intruding dyke

Where the influence of mechanically induced pore fluid pressures is added to 'static' behaviour of the full-penetration case of Fig. 19, the additional parameters of dimensionless intrusion rate U_D and dimensionless dyke width w_D exert control. Fig. 19(a) represents behaviour consistent with volcaniclastic failure zone materials. For the upper bound of $U_D = 10^0$, trends are dependent on w_D. As dyke width, w_D exceeds 10^{-1}, the influence of dyke-generated mechanically induced pore pressure increases; the stability effect of lateral restraint ($K_0 = 0{\cdot}5$) dominates behaviour of narrow blocks. For $w_D \geqslant 10^2$, three zones separated by cusps are indicated, as shown similarly for Fig. 11 and discussed above. A region of minimum stability is indicated, say $1 < d_D < 20$, but in any case the values are very low over a wide range of d_D.

For materials representative of fractured lava, $U_D = 10^{-4}$, and representative values of w_D in the range 1–10^{-3}, the influence of mechanically induced pore fluid pressure is insignificant (Fig. 19(b)). For this mechanism, dyke-generated pore fluid pressures can plausibly lead to failure in volcaniclastic material, but not in fractured lavas.

These results apply for dyke injections: for more viscous, irregular shaped intrusions injected at lower rates, as characterized by the 1980 dacite intrusion at Mount St Helens, the results would not be expected to apply.

Pore fluid pressures thermally generated by an intrusion

Parameters A_D and D govern the influence of thermal forcing on stability. For parameter groupings representing the least destabilizing thermal effect, the influence on stability is negligible (Fig. 20). Time-scales of interest include representative values of about 1 h, 4 days and 1 year. Conversely,

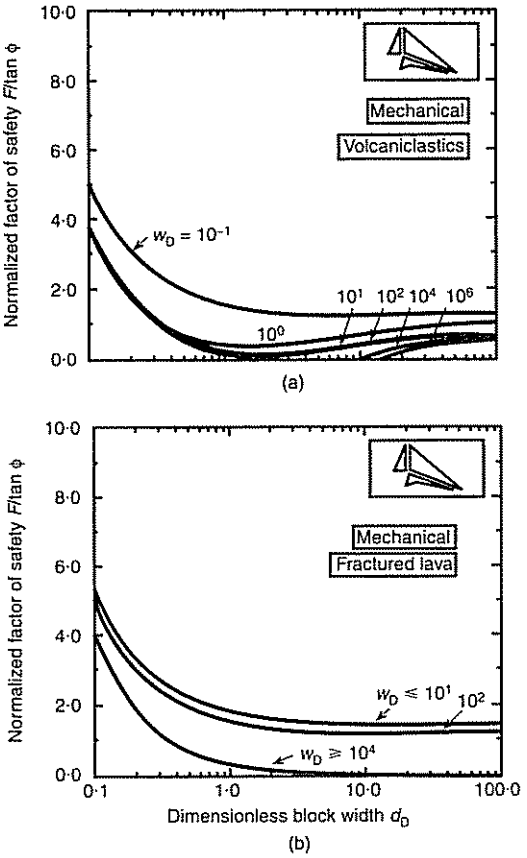

Fig. 19. Normalized factor of safety for failure of a composite volcano flank with mechanically induced pore pressures resulting from fully penetrating dyke intrusion in: (a) volcaniclastic materials; (b) fractured lava

the selection of maximum thermal forcing profoundly affects stability.

Thus under appropriate conditions, thermal straining can be an effective mechanism to enhance pore fluid pressures above ambient levels, and to initiate flank failure. Block width remains an important factor and, other factors being equal, failure is predicted for block widths $d_0 \geqslant 1$.

With block displacement following failure, the driving magma force diminishes. A limiting case is evaluated for the case where the driving magma force is wholly removed. The generally low value of $F/\tan\phi$ indicates that motion may be sustained after initial failure.

Retrograde boiling, hydrothermal processes, and earthquake-induced strength loss

As discussed above for oceanic volcanoes, the mechanical situation for extreme but nevertheless

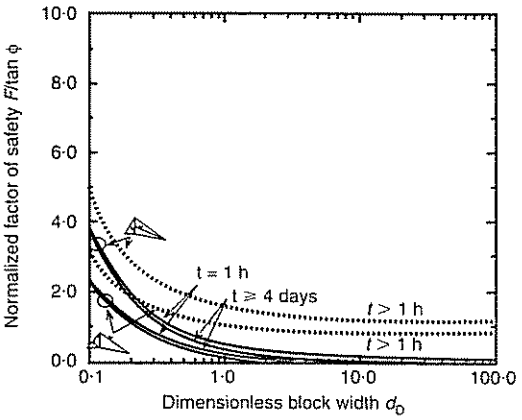

Fig. 20. Normalized factor of safety for failure of a composite volcano flank with thermally induced pore pressure resulting from a fully penetrating dyke intrusion: static piezometric conditions are variable, as noted

plausible cases approaches that shown for maximum thermal loading in Fig. 18. Deep failure is again controlled by edge loading; thus dimensionless block widths $d_D > 1$ can be generally expected, even where basal surface strength vanishes.

Additional insight is given by Fig. 21, in which generalized piezometric conditions are indicated by the ratios of total fluid uplift force on the slide plane to the normal component of total overburden weight $M \cos \alpha$. In this the pore pressure ratio r_u is defined as $r_u = \beta \cos \alpha$, where the magnitudes of β

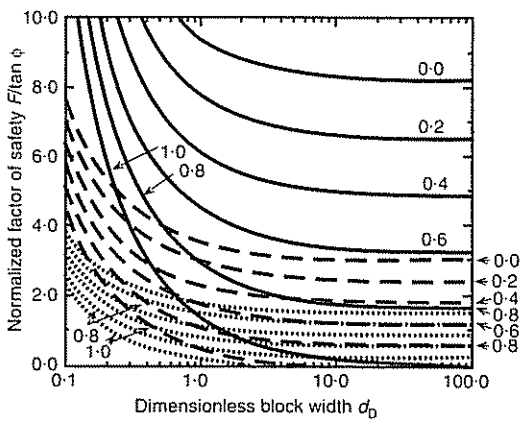

Fig. 21. Normalized factor of safety for failure of a composite volcano flank for fluid uplift ratios β of 0·0, 0·2, 0·4, 0·6, 0·8 and 1·0. These represent equivalent pore pressure ratios $r_u = \beta \cos \alpha$. Solid lines: $F_m = 0$, static loading ($\delta = 0$). Dashed lines: $F_m = 0$, dynamic loading ($\delta = 0{\cdot}2g$). Dotted lines: F_m = magmastatic loading ($\delta = 0$).

are described in Fig. 21. These generic curves may be applied to any piezometric condition irrespective of causative mechanism. The results confirm that Bezymianny-type failures, associated with magmatic pressure, are feasible with conventional piezometric conditions and nominal ϕ values. Higher fluid uplift ratios enhance the possibility of failure, and also the feasibility of failure at $d_D < 1$.

The cases for $F_m = 0$ roughly simulate Bandai-type failure, followed by phreatic explosions, or collapse lacking associated eruptions. For the static case, the data imply the need for high fluid uplift ratios ($\beta > 0{\cdot}8$). The influence of side resistance is dominant. A dramatic decrease of normalized factor of safety occurs with superposed seismic loading, where for large d_D, stability for fluid uplift ratios β of 0·4 is equivalent to static loading with a ratio β of 0·8. Where fluid pressures are already elevated by, say, hydrothermal system mechanisms, the superposition of earthquake loading can clearly trigger failure. This combination of causative factors makes the Bandai slope failure mechanically understandable, and is also consistent with the documentation of precursory seismicity and post-failure phreatic (hydrothermal) explosions.

CONCLUSIONS

The site-specific structure and stratigraphy of individual volcano flanks are paramount in any discussion of flank stability, as weak layers, heavily fissured regions, or zones with finite dimensions and specific material properties control, in all cases, the fluid pressurization and deformational response to any given set of environmental conditions and events. Thus hydrothermal systems or repetitive magmatic intrusions and eruptions are more common on volcanoes than are massive slope failures, a comparison that suggests that stringent requirements involving combinations of mechanisms and materials are necessary to produce failure. Although most intrusions, earthquakes, etc. do not cause flank failures, some clearly do so.

Thus the potential for voluminous flank failure of active volcanoes is examined. The role of magma intrusion includes several complex effects, including an important magma force that drives downslope displacements, fluid pressure forces that tend to reduce sliding resistance, and seismicity that may influence both inertial driving forces and fluid pressure components. Five pore-pressure enhancement mechanisms are noted in relation to magma emplacement, namely

(*a*) mechanical influence in poroelastic media
(*b*) thermal influence
(*c*) retrograde boiling and pressurized devolatilization of magma chambers

(*d*) hydrothermal system overpressurization, indirectly associated with magmatism
(*e*) vibrations associated with volcanic earthquakes.

Other pore-pressurization mechanisms are noted in Table 1. The seismic influence on pore-pressure may also occur with regional tectonic earthquakes.

An approach is developed to model the destabilizing influence of these pore pressures. Using materials and geometric parameters appropriate to oceanic shield volcanoes and composite volcanoes, the potential for each of these mechanisms to trigger large-scale failures is noted. For the mechanism of mechanical loading by dyke propagation, pore pressures develop close to the intrusion and result in destabilizing uplift force magnitudes that are indexed relative to intrusion rate and the width of the intrusion. For certain volcaniclastic materials the potential for failure appears feasible as a result of this triggering mechanism. However, the result is sensitive to the mechanical and hydraulic parameters assumed, and for the specific parameters representative of a particular volcano, the potential for slide initiation is not definitive.

Thermally induced pore pressures appear capable of developing large uplift forces beneath a potentially unstable block, with the disturbing magnitude related to the time since intrusion. Particularly where the dyke acts as a feeder over a sustained period of weeks, the potential to trigger failure seems clear. Likewise, under appropriate conditions the propagation of fluid pressures may occur in weak porous layers or in 'hydrofractures' as a consequence of the escape of pressurized volatiles from high-level magma chambers. A similar result may be claimed for hydrothermally generated overpressure, and for seismically generated pore fluid pressure generated in weak layers underlying volcano flanks, whether induced by local volcanic earthquakes or by large regional events. No magmatic driving force occurs in the case of Bandai-type failures, and in such cases the combination of hydrothermal-induced fluid pressurization, a fractured or alteration weakened rock mass and seismic loading may prove critical, as seems to have been the case for the type locality at Bandai, Japan.

Diverging quasi-radial boundaries commonly associated with sector collapse offer less restraint than parallel sides, and the edge resistance dissipates more rapidly with displacements. Only intrusive events of a sufficient critical severity appear capable of precipitating failure where, as a result of lateral restraint, the size of the failing block is constrained between minimum and maximum volumes. Minimum volume is conditioned by lateral frictional restraint, and maximum volume is influenced by the finite length of the intrusion that supplies the propulsive force. Similarly, the dimensions of overpressurized zones in hydrothermal systems in volcanoes control the dimensions of potential slope failure. Critical block widths for the oceanic shield type volcanoes appear in the range of kilometres to tens of kilometres, and this is consistent with evidence from the Hawaiian Islands and elsewhere; critical block widths for the composite volcanoes are smaller, as these volcanoes are themselves much smaller than oceanic volcanoes.

Once failure is initiated, driving forces due to magma pressure will drop and the potential to sustain failure must be examined in light of a sustained reduction in shear resistance. In general, the potential for the generation of large excess pore pressures along the slip zone as a result of pore contraction or collapse, or some other mechanism, appears as a necessary requirement to produce long-runout failures. Weak layers such as hyaloclastites or hydrothermally weakened tephra often can facilitate long-runout failures. Pore collapse may be catastrophic but need not be, as modest changes in porosity structure due to shear or deviatoric loading at great depth may also yield substantial generation of pore pressures, as may frictional heating. Where substantial pore pressures are available at the onset of failure, movement may be sustainable even in the absence of further pore pressure gain resulting from stress rotation and deviatoric loading in the failure zone. This is especially apparent for the uplift magnitudes feasible for sustained thermal or seismic vibration loadings. For submarine slides that surmount the pre-existing marine sediments on the submarine flank, undrained loading of these 'unstable' sediments is likely to cause a sudden drop in shear resistance of the sliding block, with the consequence that runout may be easily sustained. Consequently, the potential development of prodigious terrestrial or submarine 'debris avalanche' type landslides by these mechanisms appears feasible.

ACKNOWLEDGEMENTS

This work was supported, in part, by the National Science Foundation under grants EAR 9106134, 9117396 and 9316739, and CMS-9218547, and by the American Chemical Society under grant ACS-PRF-25922-AC2. This support is gratefully acknowledged. The authors are grateful to J. Hutchinson, an anonymous referee and an anonymous assessor of the Institution of Civil Engineers for comments that led to improvements of this paper. W. Meyer is thanked for assistance with technical data.

APPENDIX 1. DIMENSIONLESS FREE BODY FORCES

The non-dimensional forces acting on the wedge geometry of Fig. 7 are now defined. All forces have been multiplied by the quantity $d/\gamma_w h_s^3$ to yield the identities given below. These quantities represent the dimensionless block mass $\bar{M}$ as

$$\bar{M} = \tfrac{1}{2}\frac{h_m}{h_s}\frac{l}{h_s}\frac{\gamma_r}{\gamma_w}\frac{d}{h_s}$$

the dimensionless force applied by seawater loading on the submerged block toe $\bar{F}_s$ as

$$\bar{F}_s = \tfrac{1}{2}\frac{a}{h_s}\frac{l_s}{h_s}\frac{d}{h_s}$$

the dimensionless uplift force due to static groundwater pressures $\bar{F}_{ps}$ as

$$\bar{F}_{ps} = \tfrac{1}{2}\left(\frac{b}{h_s}+\frac{a}{h_s}\right)\frac{l_b}{h_s}\frac{d}{h_s}$$

and the dimensionless force applied by restraint on the lateral faces of the block $\bar{F}_{pl}$, as

$$\bar{F}_{pl} = 2\tfrac{1}{6}K_0\left(\frac{h_m^2}{h_s^2}\frac{l}{h_s}\frac{\gamma_r}{\gamma_w} - \frac{l_1}{h_s}\frac{b^2}{h_s^2}\right)$$

The magnitudes of forces exerted by magma and mechanically and thermally induced fluid pressures are dependent on the intrusion geometry. Planar dyke geometry is used in this analysis, as represented in Fig. 4.

Magma forces Total dimensionless magma force $\bar{F}_m$ acting at the rear scarp is the sum of magmastatic $\bar{F}_{ms}$ and overpressured components $\bar{F}_{mo}$, as

$$\bar{F}_m = \zeta(\bar{F}_{ms} + \bar{F}_{mo})$$

where $\zeta = \frac{1}{2}$ for mechanically induced pore pressure geometry and $\zeta = 1$ for thermally induced pore pressure geometry, with

$$\bar{F}_{ms} = \tfrac{1}{2}\frac{\gamma_m}{\gamma_w}\left(\frac{h_m}{h_s}\right)^2\frac{d}{h_s}$$

$$\bar{F}_{mo} = \frac{h_m}{h_s}\frac{h_o}{h_s}\frac{\gamma_m}{\gamma_w}\frac{d}{h_s}$$

Mechanically induced fluid pressures The dimensionless magnitude of uplift force $\bar{F}_{pm}$ generated by mechanical effects resulting from intrusion is defined as

$$\bar{F}_{pm} = \frac{w_D}{\cos\alpha}\int_{-\frac{1}{2}d_D}^{+\frac{1}{2}d_D}\int_{\frac{1}{2}U_D d_D}^{U_D R_D} K_0^*[\eta]\, e^{\eta(x_D/R_D)}\frac{R_D}{z_D}\, d\eta\, dx_D$$

where

$$U_D = \frac{U h_s}{2c}; \quad d_D = \frac{d}{h_s}$$

Thermally induced fluid pressures The dimensionless magnitude of uplift force $\bar{F}_{pt}$ generated by thermal effects resulting from magma intrusion is defined as

$$\bar{F}_{pt} = \frac{d}{h_s}\frac{A^* D K_b}{\gamma_w h_s}\frac{1}{\sqrt{\pi}}\sqrt{\left(\frac{4\kappa t}{h_s^2}\right)}\frac{1}{D\cos\alpha}$$

The corresponding geometric relationships for the wedge geometries of Figs 7 and 8 are also defined for positive α (for updip movement with failure) and negative α (for downdip movement with failure). These geometric coefficients are

$$\frac{l_b}{h_s} = \frac{h_m}{h_s}\frac{\cos\beta}{\sin(\beta+\alpha)}$$

$$\frac{l}{h_s} = \frac{l_b}{h_s}\cos\alpha$$

$$\frac{a}{h_s} = \frac{h_m}{h_s} - \frac{l_b}{h_s}\sin\alpha - 1$$

$$\frac{b}{h_s} = \frac{h_m}{h_s} - 1 + \frac{\tan\theta}{\tan\beta}$$

$$\frac{l_s}{h_s} = \frac{a}{h_s}\frac{1}{\sin\beta}$$

$$\frac{l_1}{h_s} = \frac{l}{h_s}\frac{1}{1+\frac{a}{h_s}}$$

$$\frac{l_2}{h_s} = \frac{l_s}{h_s}\sin(\alpha+\beta)$$

NOTATION

- A^* thermal strain ($\alpha_t \Delta T$)
- c hydraulic diffusivity
- d, d_D width of failing block, dimensionless block width
- D ratio of thermal to hydraulic diffusivity
- F factor of safety
- h_m, h_s magma column height at dyke contact, height of slope crest above sea level
- k intrinsic permeability
- K_0 coefficient of earth pressure at rest, $K_0 = \sigma_h/\sigma_v$
- K_0^* modified Bessel function of second kind of order zero
- K_b undrained bulk skeletal modulus of solid
- l, l_D, $\bar{l}$ length along basal failure plane, perpendicular to rear dyke, dimensionless length (l/h_s), and maximum length of basal failure plane.
- n porosity
- N normal force acting on failure plane
- p, p_s pore fluid pressure at a point, initial static pore fluid pressure and resulting induced pore fluid pressure ($p - p_s$)
- P_D^m, P_D^t dimensionless fluid pressure induced by mechanical strain (equation (2)) and by thermal strain (equation (9))
- r_u pore-pressure ratio
- R, R_D minimum radius from dyke front to point where pressure is defined, dimensionless radius (R/h_s)
- S shear force acting on failure plane
- t, t_D time since intrusion, dimensionless time
- U, U_D dyke advance rate, dimensionless advance rate
- w, w_D dyke width, dimensionless dyke width

x, y, z coordinates fixed to migrating dyke front
x_D, y_D, z_D dimensionless co-ordinates $1/h_s(x, y, z)$
α inclination of basal failure surface
α_t coefficient of free thermal expansion
β fluid uplift ratio
γ_r, γ_m, γ_w unit weight of rock, magma, water
δ seismic acceleration relative to gravity $(+\delta g)$
κ thermal diffusivity of saturated rock
μ fluid dynamic viscosity
η dummy variable of integration, equal to $U_D R_D$
ϕ angle of internal friction along failure plane

REFERENCES

Ando, M. (1979). The Hawaii earthquake of November 29, 1975: low dip angle faulting due to forceful injection of magma. *J. Geophys. Res.* **84**, 7611–7626.

Ambraseys, N. N. & Sarma, S. K. (1967). The response of earth dams to strong earthquakes. *Géotechnique* **17**, 181–213.

Anma, S., Maikuma, H., Yoshimura, M., Fujita, Y. & Okusa, S. (1988). Dynamics of earthquake-induced slope failure of Ontake. *Proc. 5th Int. Symp. Landslides. Lausanne*, 61–66.

Barton, N. R. & Choubey, V. (1977). The shear strength of rock joints in theory and practice. *Rock Mech.* **10**, No. 1, 1–54.

Belloni, L. & Morris, D. (1991). Earthquake induced shallow slides in volcanic debris soils. *Géotechnique* **41**, 439–551.

Björnsson, A., Kristjánson, L. & Johnson, H. (1977). Some observations of the Heimaey deep drill hole during the eruption of 1973. *Jökull* **26**, 52–57.

Bodvarsson, G. S., Benson, S. M., Sigurdsson, O., Stefansson, V. & Eliasson, E. T. (1984). The Krafla Geothermal Field, Iceland. 1, Analysis of well test data. *Water Resour. Res.* **20**, No. (11), 1515–1530.

Brandsdottir, B. & Einarsson, P. (1979). Seismic activity associated with the September 1977 deflation of the Krafla central volcano in northern Iceland. *J. Volcano Geotherm. Res.* **6**, 197–212.

Buchanan-Banks, J. M. (1987). Structural damage and ground failure from the November 16, 1983 Kaoiki earthquake, Island of Hawaii. In *Volcanism in Hawaii* (edited by R. W. Decker, T. L. Wright & P. H. Stauffer), professional paper 1350, pp. 1187–1195. U.S. Geological Survey.

Burnham, C. W. (1979). Magmas and hydrothermal fluids. In *Geochemistry of hydrothermal ore deposits* (edited by H. L. Barnes), 2nd edn, pp. 71–136. New York: Wiley.

Castro, G. (1975). Liquefaction and cyclic mobility of saturated sands. *J. Geotech. Engng. Div. Am. Soc. Civ. Engrs* **101**, GT6, 551–569.

Castro, G. & Poulos, S. J. (1977). Factors affecting liquefaction and cyclic mobility. *J. Geotech. Engng Div. Am. Soc. Civ. Engrs* **103** GT6, 501–506.

Cleary, M. P. (1977). Fundamental solutions for a fluid-saturated porous solid. *Int. J. Solids Struct.* **13**, 785–806.

Cleary, M. P. (1978). Moving singularities in elasto-diffusive solids with application to fracture propagation. *Int. J. Solids Struct.* **14**, 81–97.

Costa, J. E. & Schuster, R. L. (1988). The formation and failure of natural dams. *Jour. Geol. Soc. Am. Bull.* **100**, 1054–1068.

Decker, R. W. (1987). Dynamics of Hawaiian volcanoes. In *Volcanism in Hawaii* (edited by R. W. Decker, T. L. Wright & P. H. Stauffer), professional paper 1350, pp. 997–1018. U.S. Geological Survey.

Delaney, P. T. (1982). Rapid intrusion of magma into wet rock: groundwater flow due to pore pressure increases. *J. Geophys. Res.* **87**, B9, 7739–7756.

Delaney, P. T. & Pollard, D. D. (1981). *Deformation of host rocks and flow of magma during flow of minette dykes and breccia-bearing intrusions near Ship Rock, New Mexico*, professional paper 1202, pp. 1–61. U.S. Geological Survey.

Dieterich, J. T. (1988). Growth and persistence of Hawaiian volcanic rift zones. *J. Geophys. Res.* **93**, B5, 4258–4270.

Duffield, W. A., Stieltjes, L. & Varet, J. (1982). Huge landslide blocks in the growth of Piton de la Fournaise, la Reunion and Kilauea volcano, Hawaii. *J. Volcano Geotherm. Res.* **12**, 147–160.

Elsworth, D. (1991). Dislocation analysis of penetration in saturated porous media. *J. Engng Mech. Div. Am. Soc. Civ. Engrs* **117**, No. 2, 391–408.

Elsworth, D. & Piggott, A. R. (1992). Hydrofracture characterization through the monitoring of induced pore fluid pressures. *Proceedings of international conference on flow through porous media: fundamentals and reservoir engineering applications*, pp. 89–92. Moscow: Institute for Problems in Mechanics, Russian Academy of Sciences.

Elsworth, D. & Voight, B. (1992). Theory of dyke intrusion in a saturated porous solid. *J. Geophys. Res.* **97**, B6, 9105–9117.

Elsworth, D. & Voight, B. (1995). Dyke intrusion as a trigger for large earthquakes and the failure of volcano flanks. *J. Geophys. Res.* **100**, B4, 6005–6024.

Fairbridge, R. W. (1950). Landslide patterns on oceanic volcanoes and atolls. *Geograph. J.* **115**, 84–88.

Fujii, T., & Kushiro, I. (1976). Density, viscosity and compressibility of basaltic liquid at high pressures. *Carnegie Institution of Washington yearbook*, pp. 419–424.

Gilbert, P. A. (1984). *Investigation of density variation in triaxial test specimens of cohesionless soil subjected to cyclic and monotonic loading*, technical report GL 84–10. Washington, DC: U.S. Army Corps Engineers.

Goodman, R. E. & Ohnishi, Y. (1973). Undrained shear tests on jointed rock. *Rock Mech. Rock Engng* **5**, No. 3, 129–149.

Gorshkov, G. S. (1959). Gigantic eruption of the volcano Bezymianny. *Bull. Volcanol.* **21**, 77–109.

Gorshkov, G. S. (1962). On the classification and terminology of Pelée and Katmai type eruptions. *Bull. Volcanol.* **24**, 155–165.

Gucwa, P. R. & Kehle, R. O. (1978). Bearpaw Mountains rockslide, Montana, USA. *Rockslides and avalanches, 1: natural phenomena* (edited by B. Voight), pp. 393–421. Amsterdam: Elsevier.

Hall, J. (1815). On the vertical position and convolutions of certain strata, and their relation with granite. *Trans. R. Soc. Edinb.* **7**, 79–108.

Hedenquist, J. W. & Henley, R. W. (1985). Hydrothermal eruptions on the Waiotapu geothermal system, New

Zealand: their origin, associated breccias, and relation to precious metal mineralization. *Econ. Geol.* **80**, 1640–1668.

Hill, D. P. & Zucca, J. J. (1987). Geophysical constraints on the structure of Kilauea and Mauna Loa Volcanoes and some implications for seismomagmatic processes. In *Volcanism in Hawaii* (edited by R. W. Decker, T. L. Wright & P. H. Stauffer), professional paper 1350, pp. 903–917. U.S. Geological Survey.

Hoek, E. (1983). Strength of jointed rock masses. *Géotechnique* **33**, No. 3, 187–223.

Holcomb, R. T. & Searle, R. C. (1993). Large landslides from oceanic volcanoes. *Mar. Geotechnol.* **13**, 19–32.

Hubbert, M. K. & Rubey, W. W. (1959). Role of fluid pressure in mechanics of overthrust faulting. *Geol. Soc. America Bull.* **70**, 115–166.

Hutchinson, J. N. (1986). A sliding-consolidation model for flow slides. *Can. Geotech. J.* **23**, 115–126.

Hutchinson, J. N. & Bhandari, R. K. (1971). Undrained loading, a fundamental mechanism of mud flows and other mass movements. *Géotechnique* **20**, 412–438.

Iverson, R. M. (1991). Failure and runout of giant landslides on Hawaiian volcanoes: cases of enigmatic mechanics? *Geol. Soc. Am. Annu. Meeting Abstr.*, A125.

Iverson, R. M., (1992). Rigid-wedge models for metastable flanks of Hawaiian volcanoes (abstract). *EOS. Trans. Am. Geophys. Union* **73**, No. 43, 505.

Iverson, R. M. (1995). Can magma-injection and groundwater forces cause massive landslides on Hawaiian volcanoes? *J. Volcano Geotherm. Res.* **66**, 295–308.

Keefer, D. K. (1984). Landslides caused by earthquakes. *Geol. Soc. Am. Bull.* **95**, 406–421.

Kieffer, S. W. (1982). Dynamics and thermodynamics of volcanic eruptions: implications for the plumes on Io. *Satellites of Jupiter* (edited by D. Morrison), pp. 647–723. Tucson: University of Arizona Press.

Labazuy, P. & Lénat, J.-F. (1990). Recurrent landslides on the east flank of Piton de la Fournaise Volcano, Reunion. *EOS. Trans. Am. Geophys. Union Abstr.* **71**, No. 43, 1577.

Lambe, T. W. & Whitman, R. V. (1979). *Soil mechanics*. New York: Wiley.

Lénat, J.-P., Vincent, P. & Bachelery, P. (1989). The offshore continuation of an active basaltic volcano: Piton de la Fournaise (Reunion Island, Indian Ocean). *J. Volcano Geotherm. Res.* **36**, 1–36.

Lipman, P. W., Lockwood, J. P., Okamura, R. T., Swanson, D. A., & Yamashita, K. M. (1985). *Ground deformation associated with the 1975 magnitude 7.2 earthquake and resulting changes in activity of the Kilauea volcano, Hawaii*, professional paper 1276, pp. 1–45. U.S. Geological Survey.

Mink, J. F. & Lau, L. S. (1990). *Hawaiian groundwater geology and hydrogeology, and early mathematical models*, technical memorandum report 62, pp. 1–14. U.S. Geological Survey.

Moore, J. G. & Fiske, R. S. (1969). Volcanic substructure inferred from dredge samples and ocean-bottom photographs, Hawaii, *Jour. Geol. Soc. Amer. Bull.*, **80**, 1191–1202.

Moore, J. G. (1964). *Giant submarine landslides on the Hawaiian Ridge*, U.S. Geological Survey, professional paper 501-D, pp. D95–D98.

Moore, J. G. & Krivoy, H. L. (1964). The 1962 flank eruption of Kilauea volcano and structure of the east rift zone. *J. Geophys. Res.* **69**, 2033–2045.

Moore, J. G. Clague, D. A., Holcomb, R. T., Lipman, P. W., Normark, W. R. & Torresan, M. E. (1989). Prodigious submarine landslides on the Hawaiian Ridge. *J. Geophys. Res.* **94**, B12, 17465–17484.

Moriya, I. (1980). Bandaian eruption and landforms associated with it. *Collection of articles in memory of retirement of Prof. K. Nishimura from Tohoku University*, pp. 214–219 (in Japanese).

Nelson, C. E. & Giles, D. L. (1985). Hydrothermal eruption mechanisms and hot spring gold deposits. *Econ. Geol.* **80**, 1663–1639.

Newmark, N. M. (1965). Effects of earthquakes on dams and embankments. *Géotechnique* **15**, 139–159.

Okada, H. (1983). Comparative study of earthquake swarms associated with major volcanic activities. In *Arc Volcanism: physics and tectonics* (edited by D. Shimozuru, I. Yokoyama), pp. 43–61. Tokyo: Terra Science.

Ouyang, Z. (1994). *An investigation of dislocations propagating in poroelastic media*. PhD thesis, Pennsylvania State University, University Park.

Oyagi, N. (1987). The 1984 Ontake-san landslide and its movement. *Trans. Jpn. Geomorphol. Union* **8**, No. 2, 127–144.

Pariseau, W. G. & Voight, B. (1979). Rockslides and avalanches: basic principles and perspectives in the realm of civil and mining operations. In *Rockslides and avalanches, 2: engineering sites* (edited by B. Voight), pp. 1–92. Amsterdam: Elsevier.

Prostka, H. J. (1978). Heart Mountain fault and Absaroka volcanism. In *Rockslides and avalanches, 1: natural phenomena* (edited by B. Voight), pp. 423–437. Amsterdam: Elsevier.

Rice, J. R. & Cleary, M. P. (1976). Some basic stress diffusion solutions for fluid-saturated elastic porous media with compressible constituents. *Rev. Geophys.* **14**, No. 2, 227–241.

Romagnoli, C. and Tibaldi, A. (1994). Volcanic collapse in different tectonic setting: an example from the Aeolian Arc, Italy. Abstract volume, *Conference on volcanic instability on the earth and other planets*. Geological Society of London.

Rubin, A. M. & Pollard, D. D. (1987). Origins of blade-like dykes in volcanic rift zones. In *Volcanism in Hawaii* (edited by R. W. Decker, T. L. Wright & P. H. Stauffer), professional paper 1350, pp. 1449–1470. U.S. Geological Survey.

Rudnicki, J. W. (1981). On 'Fundamental solutions for a fluid-saturated porous solid' by M. P. Cleary. *Int. J. Solids Struct.* **17**, 855–857.

Sassa, K. (1988). Geotechnical model for the motion of landslides. *Proc. 5th Int. Symp. Landslides, Lausanne*.

Seed, H. B. (1979). Considerations in the earthquake-resistant design of earth and rockfill dams. *Géotechnique* **29**.

Seed, H. B. (1981). Earthquake-resistant design of earth dams. *Proceedings of international conference on recent advances in geotechnical earthquake engineering and soil dynamics*, University of Missouri, Rolla, vol. 3, pp. 1157–1175.

Seed, H. B., Lee, K. L. & Idriss, I. M. (1969). Analysis of Sheffield dam failure. *J. Soil Mech. Fdn Engng Div. Am. Soc. Civ. Engrs* **95**, 1453–1490.

Sekiya, S. & Kikuchi, Y. (1889). The eruption of Bandai-san. *Tokyo Imp. Univ. Coll. Sci. J.* **3**, No. 2, 91–172.

Siebert, L. (1984). Large volcanic debris avalanches: characteristics of source areas, deposits, and associated eruptions. *J. Volcano Geotherm. Res.* **22**, 163–197.

Siebert, L., Glicken, H. & Ui, T. (1987). Volcanic hazards for Bezymianny- and Bandai-type eruptions. *Bull. Volcanol.* **49**, 435–459.

Sigurdsson, O. (1982). Analysis of pressure pulses resulting from volcanic activity in the vicinity of a well. (Misc. thesis). University of Oklahoma, Norman, Oklahoma, 75 pp.

Skempton, A. W. (1954). The pore-pressure coefficients *A* and *B*. *Géotechnique* **4**, 143–147.

Slingerland, R. & Voight, B. (1979). Occurrence, properties, and predictive models of landslide-generated water waves. In *Rockslide and Avalanche 2: Engineering Sites* (edited by B. Voight), 317–397. Amsterdam: Elsevier.

Sousa, J. & Voight, B. (1991). Continuum simulation of flow failure. *Géotechnique* **41**, 515–538.

Sousa, J. & Voight, B. (1995). Multiple-pulsed debris avalanche emplacement at Mount St. Helens in 1980: evidence from numerical continuum flow simulation. *J. Volcano Geotherm. Res.* **66**, 1–99.

Stearns, H. T. & MacDonald, G. A. (1946). Geology and groundwater resources of the island of Hawaii. *Hawaii Div. Hydrogr. Bull.* **9**.

Stefánsson, V. (1981). The Krafla geothermal field, northern Iceland. In *Geothermal systems: principles and case histories* (edited by L. Rybach & L. J. P. Muffler), pp. 273–294. New York: Wiley.

Swanson, D. A., Duffield, W. A. & Fiske, R. S. (1976). *Displacement of the south flank of Kilauea volcano: the result of forceful intrusion of magma into the rift zones*, professional paper 963, pp. 1–30. U.S. Geological Survey.

Taylor, D. W. (1948). Fundamentals of soil mechanics. New York: Wiley.

Terzaghi, K. (1950). Mechanisms of landslides. In *Application of geology to engineering practice* (edited by S. Paige), pp. 83–123. Washington, D.C.: Geological Society of America.

Thomas, D. (1987). A geochemical model of the Kilauea east rift zone. In *Volcanism in Hawaii* (edited by R. W. Decker, T. L. Wright & P. H. Stauffer), professional paper 1350, pp. 1507–1525. U.S. Geological Survey.

Tilling, R. I., Koyanagi, R. Y., Lipman, P. W., Lockwood, J. P., Moore, J. G., & Swanson, D. A. (1976). *Earthquakes and related catastrophic events, Island of Hawaii, November 29, 1975: a preliminary report*, circular 740. U.S. Geological Survey.

Tryggvason, E. (1980). Subsidence events in the Krafla area, north Iceland, 1975–1979. *J. Geophysics* **47**, 141–153.

Varnes, D. J. (1978). Slope movement types and processes. In *Landslides, analysis and control*, (edited by R. L. Schuster & R. J. Krizek), pp. 11–35. Washington, D.C.: National Academy of Sciences.

Voight, B. (1972). Fluid-wedge hypothesis and the Heart Mountain and Reef Creek decollements, northwestern Wyoming, USA. *Geol. Soc. Am. Abstr. Programs* **4**, 698.

Voight, B. (1974). Thin-skinned graben, plastic wedges, and deformable plate tectonics. In *Approaches to taphrogenesis*, Inter-Union Commission on Geodynamics, science report **8**, pp. 395–419. Stuttgart: E. Schweizerbartsche Verlagsbuchhandlung.

Voight, B. (1976). *Mechanics of thrust faults and decollement*. Stroudsburg, PA: Dowden, Hutchinson & Ross.

Voight, B. (ed.) (1978). Rockslides and avalanches 1: natural phenomena. Amsterdam: Elsevier.

Voight, B. (ed.) (1979). Rockslides and avalanches 2: engineering sites. Amsterdam: Elsevier.

Voight, B. (1992). Causes of landslides: conventional factors and special considerations for geothermal sites and volcanic regions. *Geotherm. Resour. Counc. Trans.* **16**, 529–533.

Voight, B. & Elsworth, D. (1992). Resolution of mechanics problems for prodigious Hawaiian landslides: magmatic intrusions simultaneously increase driving force and decrease driving resistance by fluid pressure enhancement. *EOS, Trans. Am. Geophys. Union* **73**, No. 43, 506.

Voight, B. & Faust, C. (1979). Heat-induced fluid pressure enhancement mechanism in seismic faulting. *EOS, Trans. Am. Geophys. Union*, abstract, 60.

Voight, B. & Faust, C. (1982). Frictional heat and strength loss in some rapid landslides. *Géotechnique* **32**, 43–54.

Voight, B. & Faust, C. (1992). Friction heat and strength loss in some rapid landslides: correction and affirmation of mechanism at Vaiont landslide. *Géotechnique* **42**, 641–643.

Voight, B., Janda, R. J., Glicken, H. & Douglass, P. M. (1983). Nature and mechanics of the Mount St. Helens rockslide-avalanche of 18 May 1980. *Géotechnique* **33**, 243–273.

Voight, B. & Sousa, J. (1994). Lessons from Ontake-san: a comparative analysis of debris avalanche dynamics. *Engng Geol.* **38**, 261–297.

Watanabe, H. (1983). Changes in water level and their implications to the 1977–1978 activity of Usu volcano. *Arc volcanism: physics and tectonics* (edited by D. Shimozuru & J. Yokoyama), pp. 81–93. Tokyo: Terra Science.

Wohletz, K. & Heiken, G. (1992). *Volcanology and geothermal energy*. Berkeley: University of California Press.

Ylinen, A. M. & Elsworth, D. (1991). Heat and mass transfer around an advancing penetrometer. *Int. J. Heat Mass Transfer* **34**, No. 6, 1407–1416.

Yonechi, F. (1987). A new hypothesis on the collapse of Bandai-san Volcano in 1888. *Sci Rep Tohoku Univ., 7th Series (Geogr.)* **37**, 159–173.

Zucca, J. J. & Hill, D. P. (1980). Crustal structure of the southeast flank of Kilauea Volcano, Hawaii, from seismic refraction measurements. *Bull. Seismol. Soc. Am.* **70**, 1149–1159.

Zucca, J. J., Hill, D. P. & Kovach, R. L. (1982). Crustal structure of Mauna Loa Volcano, Hawaii, from seismic refraction measurements and gravity data. *Bull. Geol. Soc. Am.* **72**, 1535–1550.